



*Supplement of*

## **Aerosol characterization over the southeastern United States using high resolution aerosol mass spectrometry: spatial and seasonal variation of aerosol composition, sources, and organic nitrates**

**L. Xu et al.**

*Correspondence to:* N. L. Ng ([ng@chbe.gatech.edu](mailto:ng@chbe.gatech.edu))

24       The selection of optimal solutions for PMF analysis on merged organic and nitrate mass  
25 spectra (i.e.,  $\text{PMF}_{\text{org+NO}_3}$ ) is mainly based on comparing the time series (Fig. S5), mass spectrum  
26 (Fig. S5), and campaign-average mass concentration (Fig. S6) with factors from PMF analysis on  
27 organic mass spectra only (i.e.,  $\text{PMF}_{\text{org}}$ ), in addition to examining the typical diagnostic plots  
28 (Fig. S3). Based on the identification of a nitrate inorganic aerosol (NIA) factor, we divide all  
29 seven datasets into two categories: 1) CTR\_June and YRK\_July where a NIA factor is not  
30 resolved and 2) the other sites where a NIA factor is resolved.

31       For CTR\_June and YRK\_July, the same factors are resolved from  $\text{PMF}_{\text{org+NO}_3}$  analysis as  
32 those from  $\text{PMF}_{\text{org}}$  analysis. The factors from  $\text{PMF}_{\text{org+NO}_3}$  show good correlation with  
33 corresponding factors from  $\text{PMF}_{\text{org}}$  regarding both time series ( $R>0.964$ ) and mass spectrum  
34 ( $R>0.997$ ) (Fig. S5).

35       We note that in the optimal solutions of CTR\_June and YRK\_July, the residuals of  $\text{NO}^+$   
36 and  $\text{NO}_2^+$  (i.e.,  $\sum(\text{Resid}^2/\sigma^2)/Q_{\text{exp}}$ ) are larger than that in the optimal solutions of other sites  
37 where NIA factor is resolved (Fig. S3). If one goes to higher number factor solutions, the  
38 residuals of  $\text{NO}^+$  and  $\text{NO}_2^+$  of CTR\_June and YRK\_July are reduced, but the correlations  
39 between factors from  $\text{PMF}_{\text{Org+NO}_3}$  and corresponding factors from  $\text{PMF}_{\text{Org}}$  are weakened and  
40 splitting behavior of real factors occurs (Ulbrich et al., 2009). Take YRK\_July for example, the  
41 residual of  $\text{NO}^+$  decreases from 155 in the three-factor solution (Fig. S3(c)) to 31 in the five-  
42 factor solution (Fig. S17). However, the correlations of the time series between factors from  
43  $\text{PMF}_{\text{Org+NO}_3}$  and the corresponding factors from  $\text{PMF}_{\text{Org}}$  are all weakened (Fig. S18 and Fig. S5).  
44 In addition, MO-OOA in three-factor solution splits into two factors in five-factor solution. Thus,  
45 we select three-factor solution as the optimal solution for YRK\_July in the  $\text{PMF}_{\text{Org+NO}_3}$  analysis.

46       For all the sites except CTR\_June and YRK\_July, a nitrate inorganic aerosol (NIA) factor  
47 was resolved. All OA factors except LO-OOA from  $\text{PMF}_{\text{org+NO}_3}$  show good correlation with the  
48 corresponding  $\text{PMF}_{\text{org}}$  OA factors with  $R>0.89$  for time series and  $R>0.98$  for mass spectrum  
49 (Fig. S5). The correlation of the LO-OOA time series obtained from  $\text{PMF}_{\text{org+NO}_3}$  and  $\text{PMF}_{\text{org}}$   
50 analysis ranges from 0.77 to 0.98 (Fig. S5), which is not as strong as the correlation of other OA  
51 factors. This is likely due to that the time series of LO-OOA being more similar to the total  
52 measured nitrate (i.e.,  $\text{NO}_{3,\text{meas}}$ ) than other OA factors, so that PMF has difficulty in separating  
53 LO-OOA and NIA factor.

54 A FPEAK value of 0 is chosen for all datasets except RS\_Jan. For RS\_Jan dataset,  
55 PMF<sub>org+NO<sub>3</sub></sub> solution with FPEAK = 0.2 is selected due to the following reasons. First of all,  
56 solution with FPEAK=0 is not converged. Second of all, solution with FPEAK = 0.2 provides  
57 the best correlation with PMF<sub>org</sub> factors for all the OA factors from PMF<sub>org+NO<sub>3</sub></sub> analysis. For  
58 example, PMF<sub>org+NO<sub>3</sub></sub> solution with FPEAK =-0.2 cannot resolve a clear LO-OOA factor as  
59 shown in Fig. S19.

60 Unlike all the other sites where all PMF<sub>org</sub> OA factors can be clearly resolved in the  
61 corresponding PMF<sub>org+NO<sub>3</sub></sub> analysis, we cannot resolve MO-OOA factor from PMF<sub>org+NO<sub>3</sub></sub> for  
62 YRK\_Dec even up to ten-factor solution. From PMF<sub>org</sub> analysis on YRK\_Dec, we resolved three  
63 factors, which are MO-OOA, LO-OOA, and BBOA. For PMF<sub>org+NO<sub>3</sub></sub> on YRK\_Dec, in the two-  
64 factor solution, we resolve one NIA factor and only one OA factor, indicating that a two-factor  
65 solution is insufficient to separate BBOA and OOA factors. In the three-factor solution, we  
66 resolve clear NIA and BBOA factors, but just one OOA factor. This OOA factor correlates well  
67 with the combined LO-OOA and MO-OOA factors from PMF<sub>org</sub> three-factor solution ( $R=0.94$ )  
68 (Fig. S20(b)), indicating the OOA factor from PMF<sub>org+NO<sub>3</sub></sub> three-factor solution likely represents  
69 the combination of LO-OOA and MO-OOA from PMF<sub>org</sub> three-factor solution. In PMF<sub>org+NO<sub>3</sub></sub>  
70 four-factor solution, we resolve a factor whose correlation with all factors from PMF<sub>org</sub> is very  
71 weak (i.e., the highest R is 0.63) (Fig. S20(c)). This suggests that “splitting” behavior occurs for  
72 the PMF<sub>org+NO<sub>3</sub></sub> four-factor solution. Taken together, PMF<sub>org+NO<sub>3</sub></sub> with a three-factor solution is  
73 optimal for YRK\_Dec. It is also important to note that the focus of PMF<sub>org+NO<sub>3</sub></sub> is for nitrate  
74 source apportionment. Although PMF<sub>org+NO<sub>3</sub></sub> resolves different OA factors for different solutions,  
75 the concentration of the NIA factor remains almost constant (i.e., the NIA factor concentration  
76 ranges from 0.54 - 0.6  $\mu\text{g}/\text{m}^3$  from 2 to 5 factor solutions). Thus, the number of factors resolved  
77 for YRK\_Dec has minimal effect on our conclusion.

78

79

80

81

82

83 **Figure Captions**

84

85 Fig. S1. Diagnostic plots of the PMF analysis on the high-resolution organic mass spectra (i.e.,  
86  $\text{PMF}_{\text{org}}$  analysis). The following plots are shown for all the datasets: (1)  $Q/Q_{\text{exp}}$  vs number of  
87 factors; (2)  $Q/Q_{\text{exp}}$  vs. FPEAK for the solution with optimal number of factors; (3) mass fraction  
88 of PMF factors vs. FPEAK; (4) correlations of time series and mass spectra among PMF factors;  
89 (5) the distribution of scaled residuals for each  $m/z$ ; (6) the time series of the measured and the  
90 reconstructed organic mass; (7) variations of the residual (= measured - reconstructed) of the  
91 least-square-fit vs. time; (8) the time series of  $Q/Q_{\text{exp}}$ ; (9) the  $Q/Q_{\text{exp}}$  values vs.  $m/z$ .

92 Fig. S2. The mass spectra and time series of OA factors resolved from PMF analysis on the high-  
93 resolution organic mass spectra (i.e.  $\text{PMF}_{\text{org}}$  analysis). The mass spectra are colored by ion type.

94 Fig. S3. Diagnostic plots of the PMF analysis on the high-resolution merged organic and nitrate  
95 mass spectra (i.e.  $\text{PMF}_{\text{org+NO}_3}$  analysis). The following plots are shown for all the datasets: (1)  
96  $Q/Q_{\text{exp}}$  vs. number of factors; (2)  $Q/Q_{\text{exp}}$  vs FPEAK for the solution with optimal number of  
97 factors; (3) mass fraction of PMF factors vs. FPEAK; (4) correlations of time series and mass  
98 spectra among PMF factors; (5) the distribution of scaled residuals for each  $m/z$ ; (6) the time  
99 series of the measured and the reconstructed organic mass; (7) variations of the residual (=  
100 measured - reconstructed) of the least-square-fit vs. time; (8) the time series of  $Q/Q_{\text{exp}}$ ; (9) the  
101  $Q/Q_{\text{exp}}$  values vs.  $m/z$ .

102 Fig. S4. The mass spectra and time series of OA factors resolved from PMF analysis on the high-  
103 resolution merged organic and nitrate mass spectra (i.e.  $\text{PMF}_{\text{org+NO}_3}$  analysis). The mass spectra  
104 are colored by ion type.

105 Fig. S5. Mass spectra and time series comparison of factors resolved from PMF analysis on  
106 merged organic and nitrate mass spectra (i.e.  $\text{PMF}_{\text{org+NO}_3}$ ) and factors resolved from PMF  
107 analysis on organic mass spectra (i.e.  $\text{PMF}_{\text{org}}$ ).

108 Fig. S6. The campaign-average mass concentration comparison of factors resolved from PMF  
109 analysis on merged organic and nitrate mass spectra (i.e.  $\text{PMF}_{\text{org+NO}_3}$ ) and factors resolved from  
110 PMF analysis on organic mass spectra (i.e.  $\text{PMF}_{\text{org}}$ ). RIE and CE are not applied.

111 Fig. S7. The campaign average mass spectra of total OA for all datasets. The mass spectra are  
112 colored by ion type.

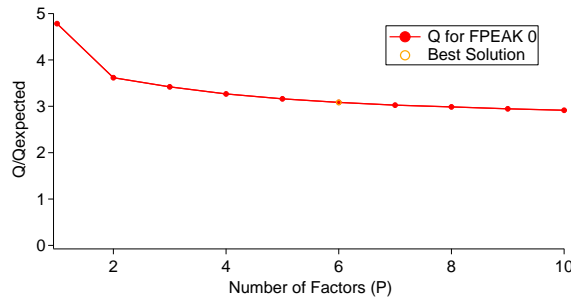
113 Fig. S8. The diurnal profiles of brown carbon for all the datasets.

114 Fig. S9. The scatter plot of Isoprene-OA and brown carbon for the datasets where Isoprene-OA  
115 factor is resolved.

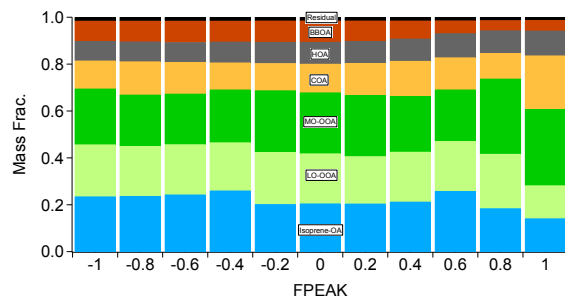
- 116 Fig. S10. The atomic O:C and H:C ratios of OA factors resolved from PMF analysis on high-  
117 resolution organic mass spectra (i.e.  $\text{PMF}_{\text{org}}$ ).
- 118 Fig. S11. The mass fraction of nitrate signals (i.e.,  $\text{NO}^+$  and  $\text{NO}_2^+$ ) and organic signals in the  
119 nitrate inorganic aerosol (NIA) factor for the datasets where this factor is resolved.
- 120 Fig. S12. The  $\text{NO}^+/\text{NO}_2^+$  ratio of the nitrate inorganic aerosol (NIA) factor resolved from PMF  
121 analysis on merged organic and nitrate mass spectra (i.e.  $\text{PMF}_{\text{org+NO}_3}$  analysis) normalized by the  
122  $\text{NO}^+/\text{NO}_2^+$  ratio of ammonium nitrate of each dataset.
- 123 Fig. S13. The time series of sodium and nitrate measured by a PILS-IC at Centreville, AL. The  
124  $\text{PM}_{2.5}$  cyclone was replaced with a  $\text{PM}_1$  cyclone on June 24<sup>th</sup>, 2013.
- 125 Fig. S14. The relationship between ACSM measurements (stationary at the Georgia Tech site)  
126 and HR-ToF-AMS measurements (rotating among different sites) of NR- $\text{PM}_1$  species.
- 127 Fig. S15. The diurnal profiles of  $R_{\text{meas}}/R_{\text{AN}}$  for all datasets.
- 128 Fig. S16. The diurnal profile of total measured  $\text{NO}_3$  (i.e.,  $\text{NO}_{3,\text{meas}}$ ), estimated  $\text{NO}_3$  from  
129 inorganic nitrate and organic nitrate (i.e.,  $\text{NO}_{3,\text{inorg}}$  and  $\text{NO}_{3,\text{org}}$ , respectively) by using the  $\text{NO}_x^+$   
130 ratio method with a  $R_{\text{ON}}$  value of 10.
- 131 Fig. S17. The Q/Qexp values for each  $m/z$  of YRK\_July PMF<sub>org+NO<sub>3</sub></sub> five-factor solution.
- 132 Fig. S18. Time series comparison of PMF<sub>org+NO<sub>3</sub></sub> five-factor solution and PMF<sub>org</sub> for YRK\_July.
- 133 Fig. S19. Time series comparison of PMF<sub>org+NO<sub>3</sub></sub> six-factor solution with FPEAK = -0.2 and  
134 PMF<sub>org</sub> for RS\_Jan.
- 135 Fig. S20. Time series comparison of PMF<sub>org+NO<sub>3</sub></sub> and PMF<sub>org</sub> for YRK\_Dec.
- 136
- 137
- 138
- 139
- 140
- 141
- 142
- 143

144 Fig. S1.

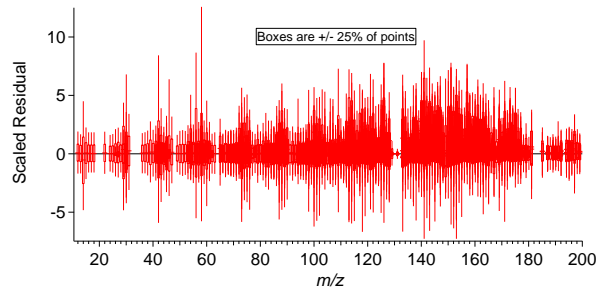
145 a) JST\_May



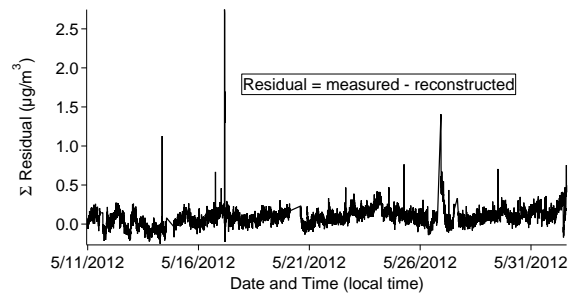
146



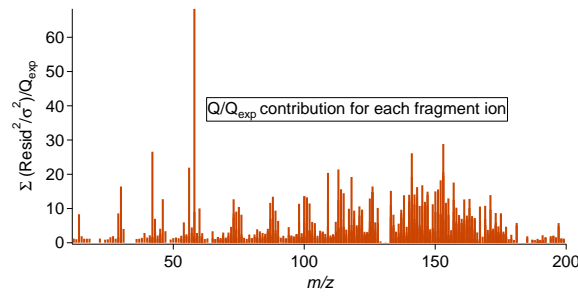
147



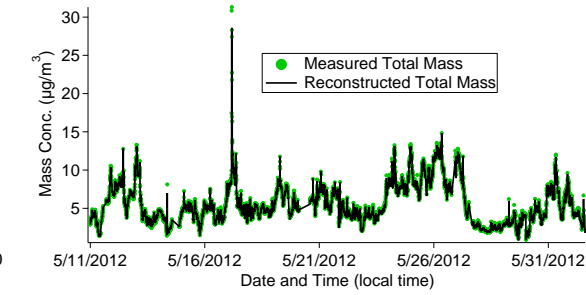
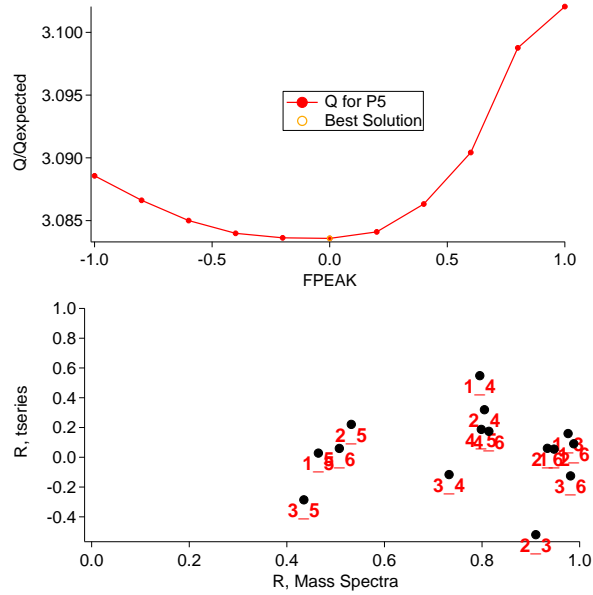
148



149

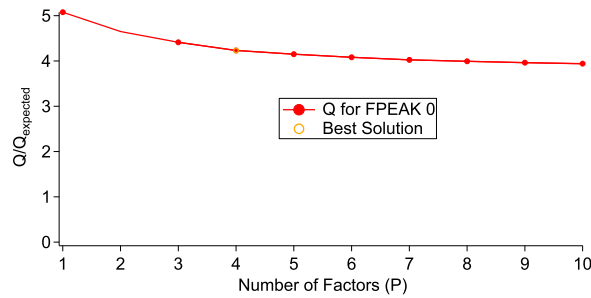


150

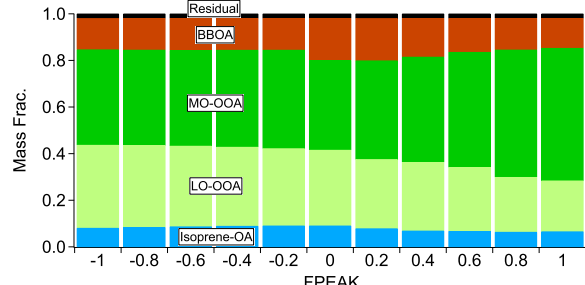


151

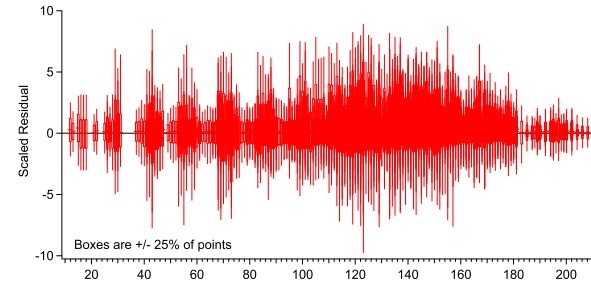
152 b) CTR\_June



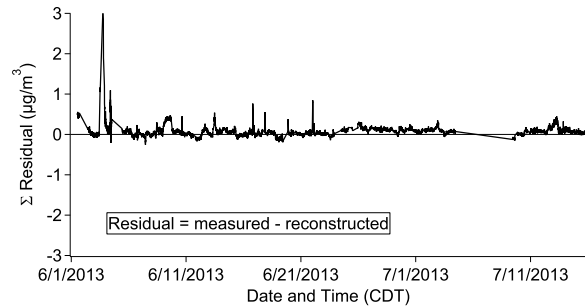
153



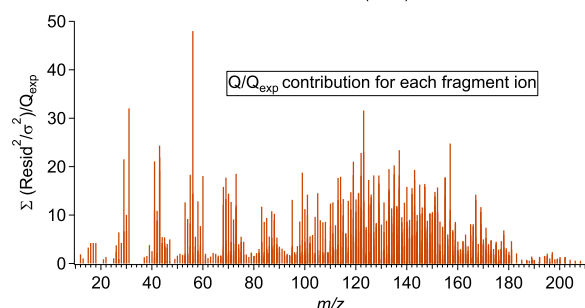
154



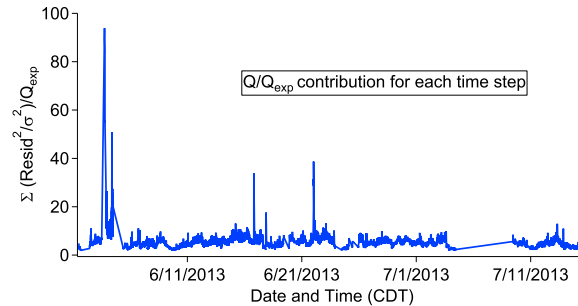
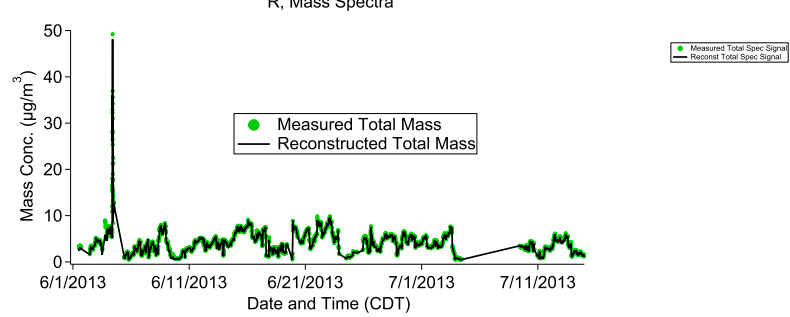
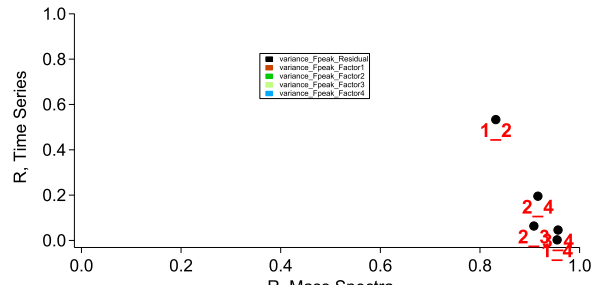
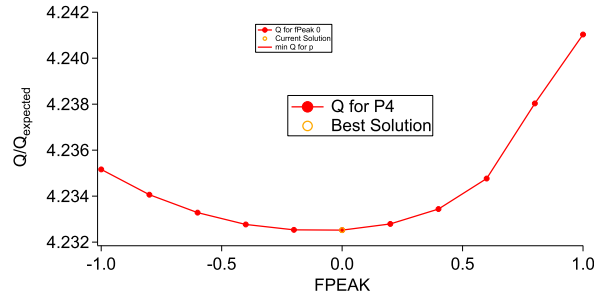
155



156

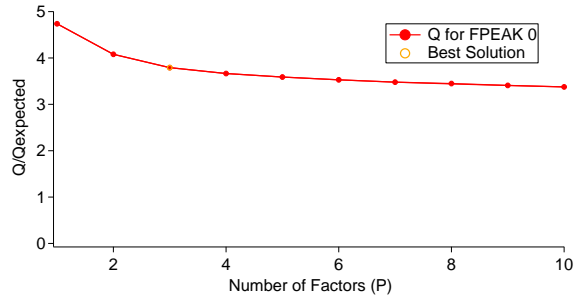


157

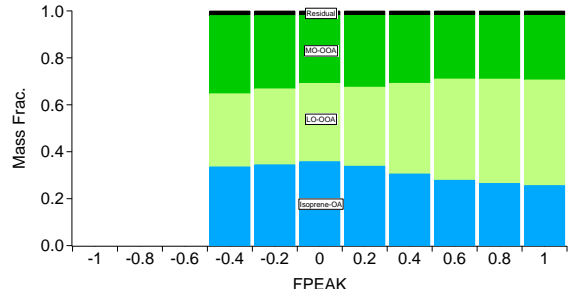


158

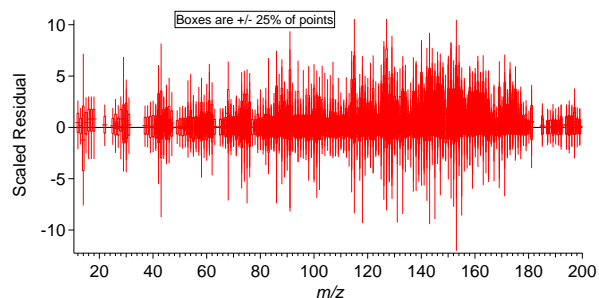
159 c) YRK\_July



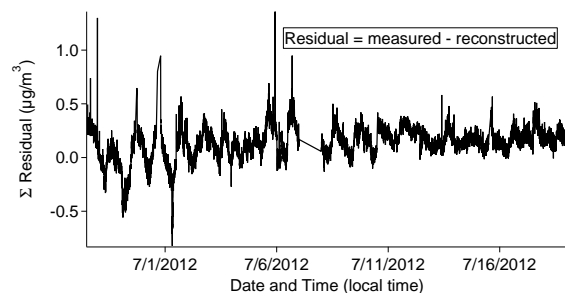
160



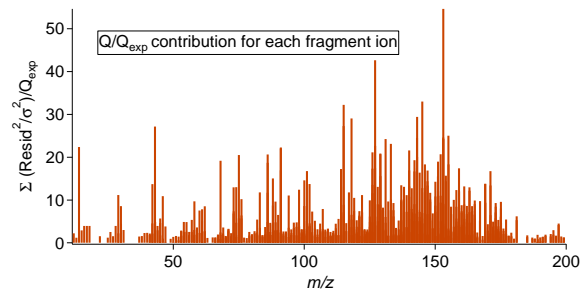
161



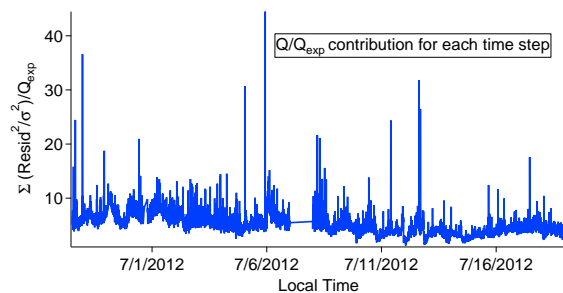
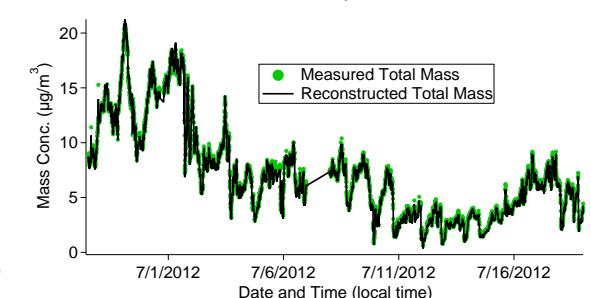
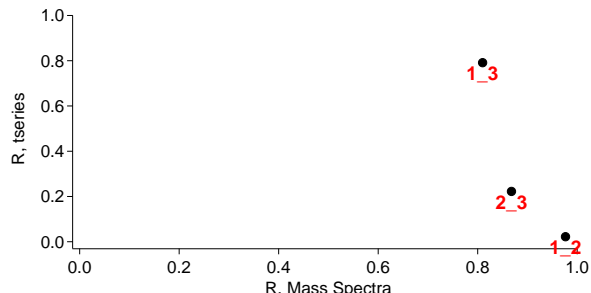
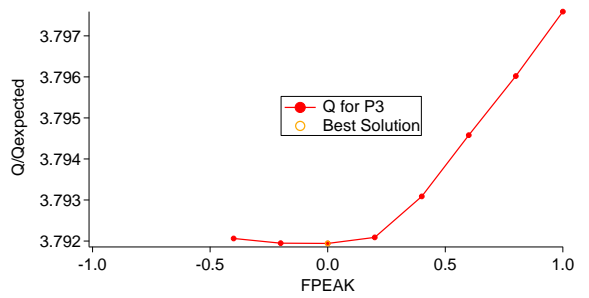
162



163



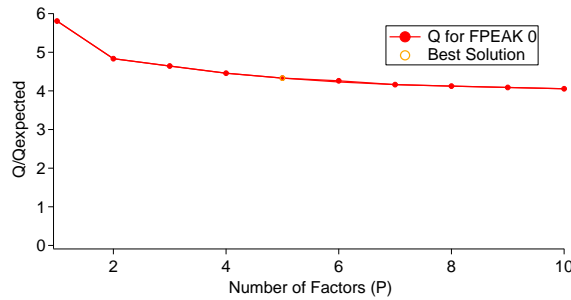
164



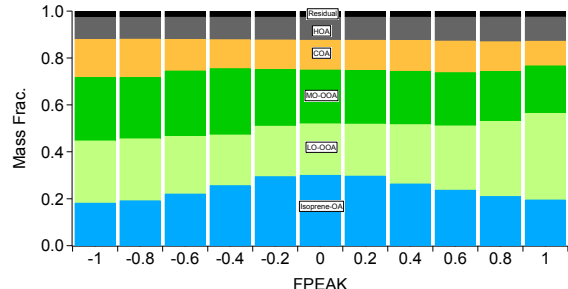
165

166

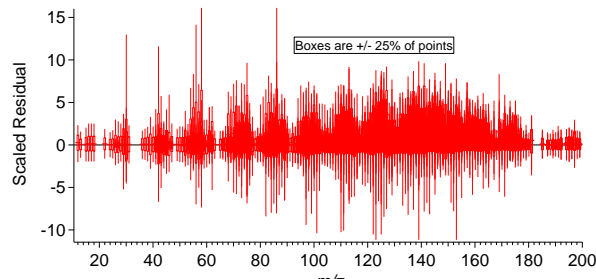
167 d) GT\_Aug



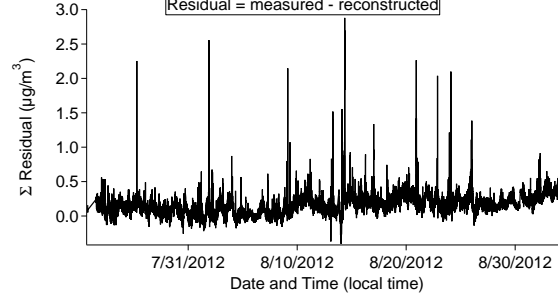
168



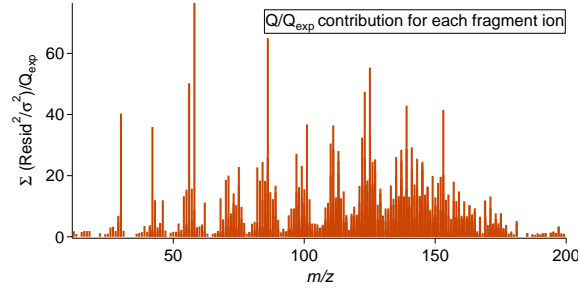
169



170



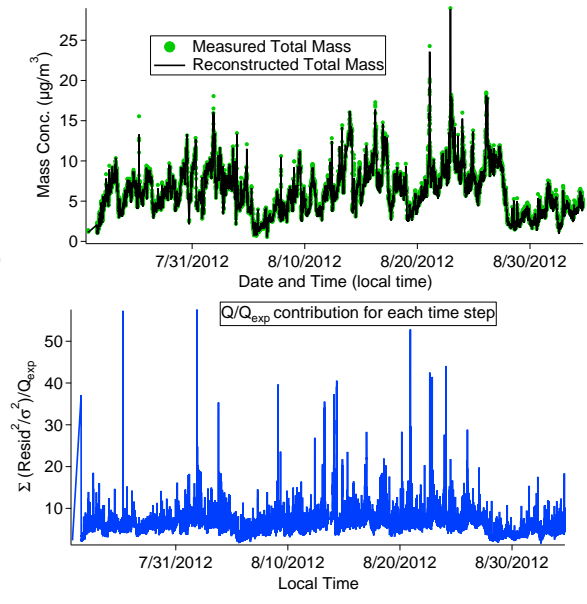
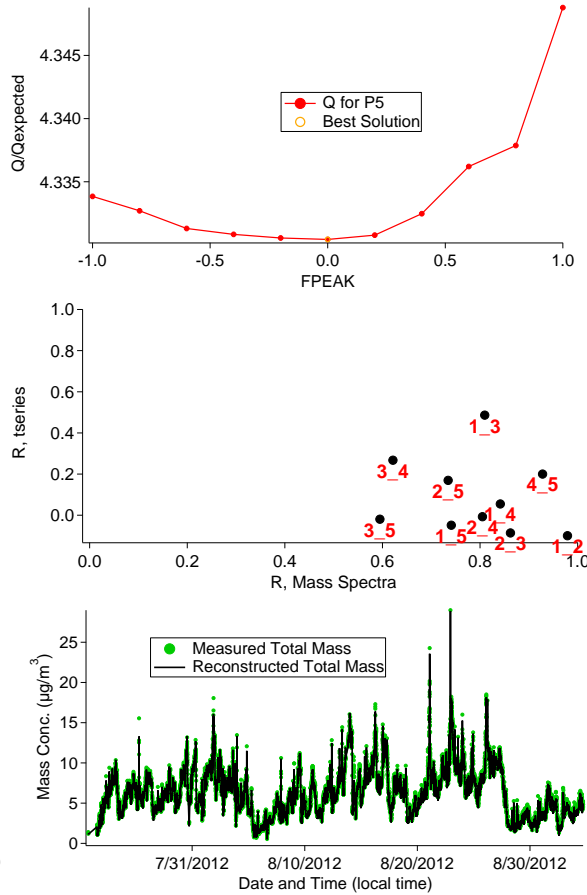
171



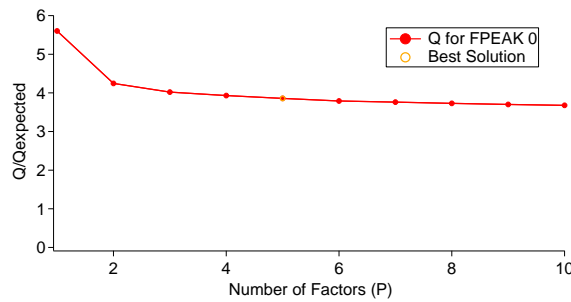
172

173

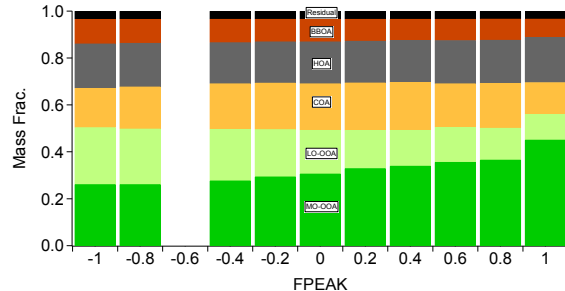
174



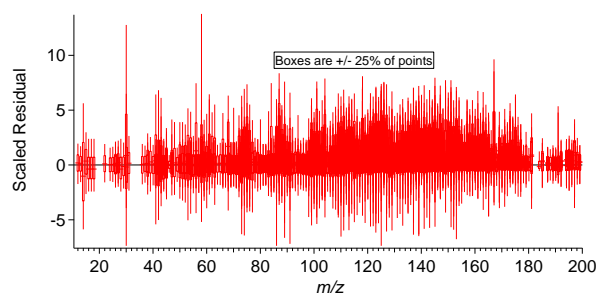
175 e) JST\_Nov



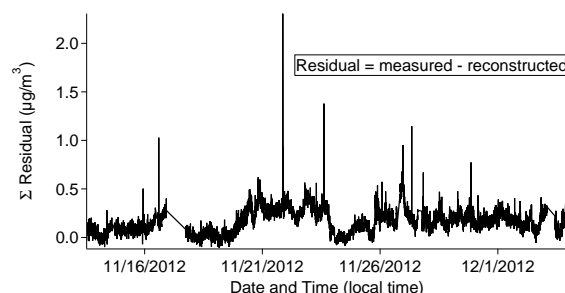
176



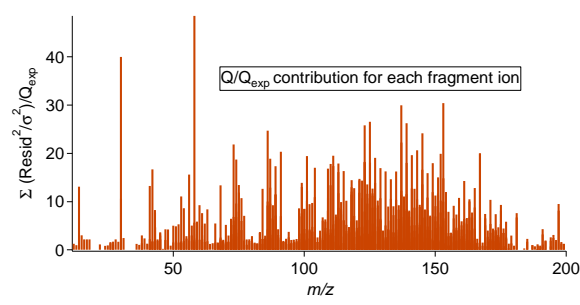
177



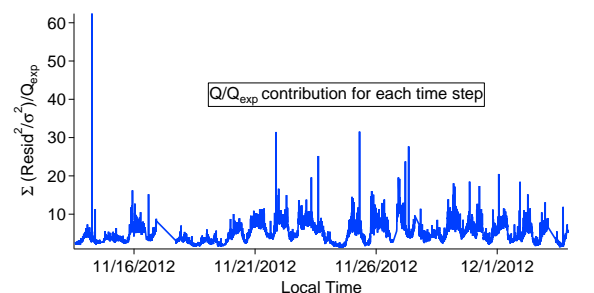
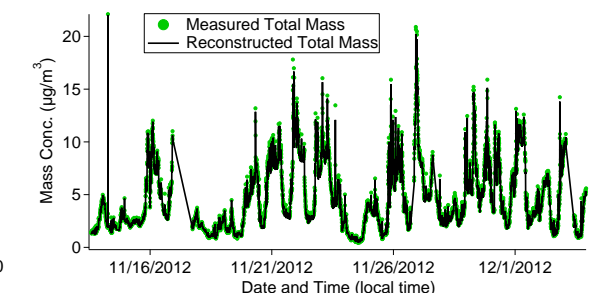
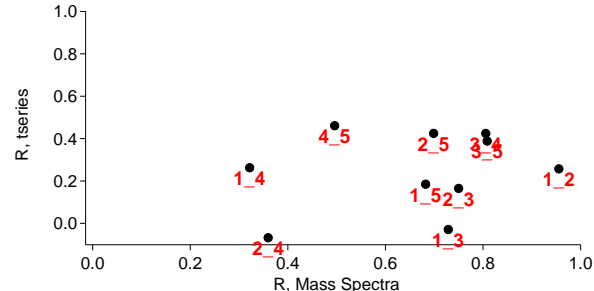
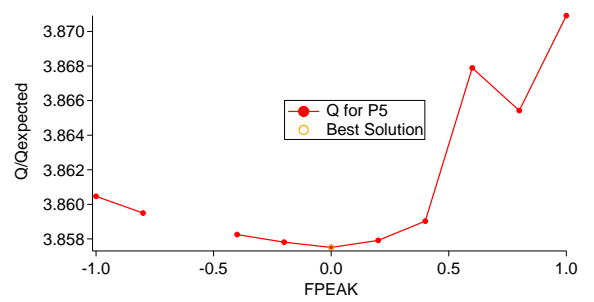
178



179



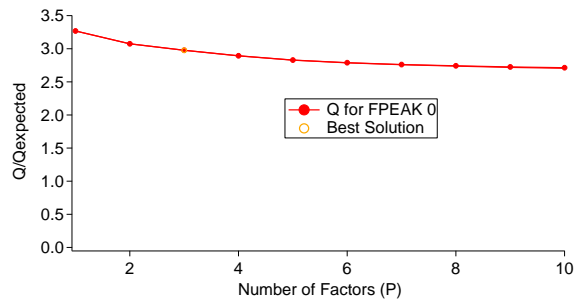
180



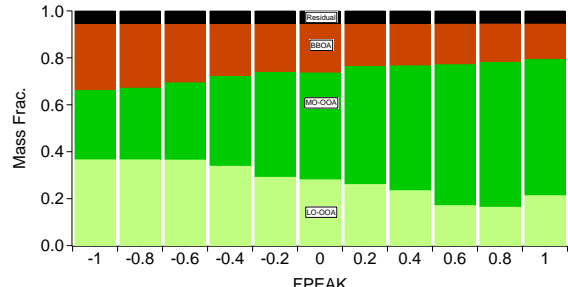
181

182

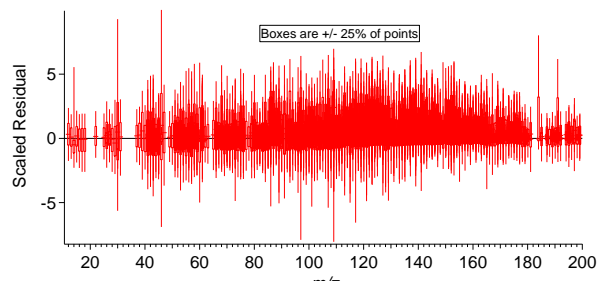
183 f) YRK\_Dec



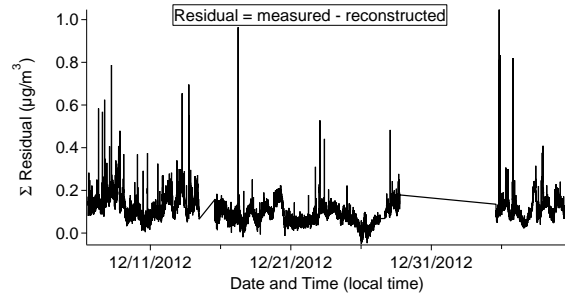
184



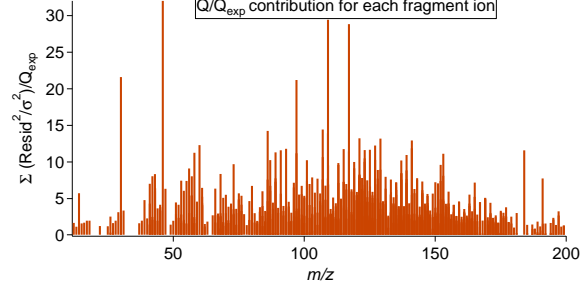
185



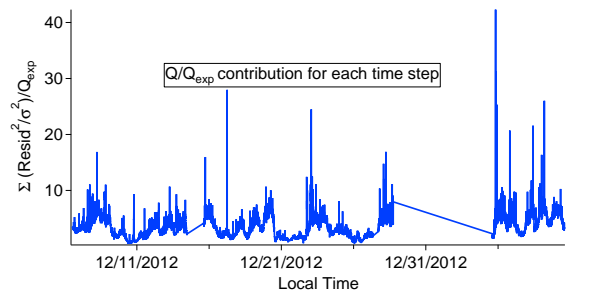
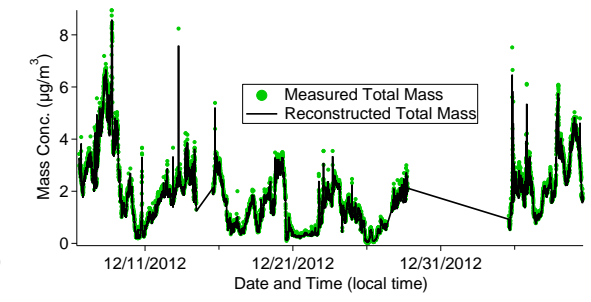
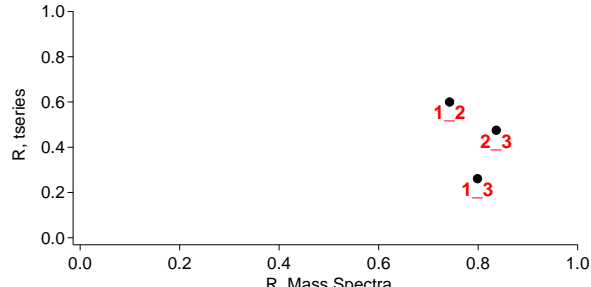
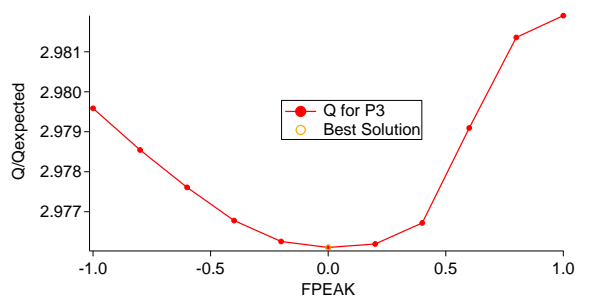
186



187



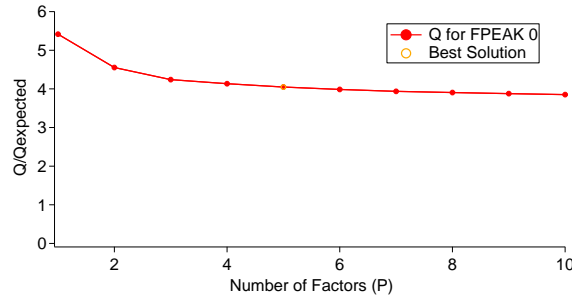
188



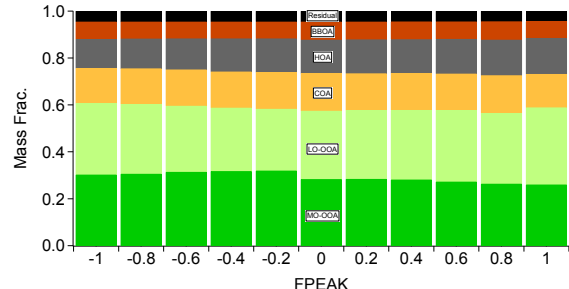
189

190

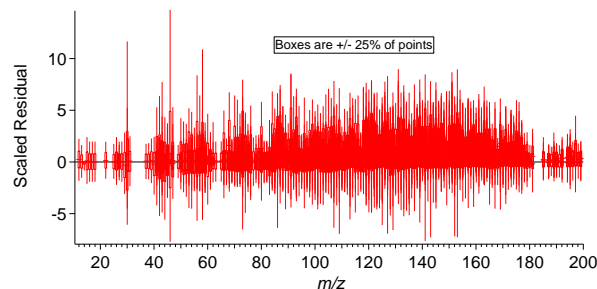
191 g) RS\_Jan



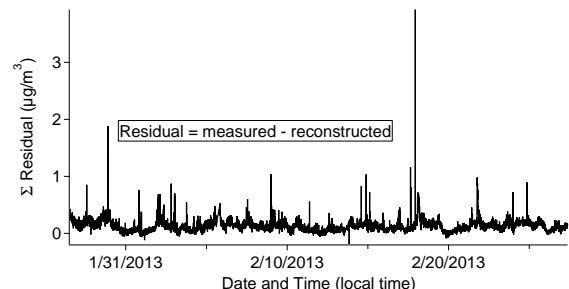
192



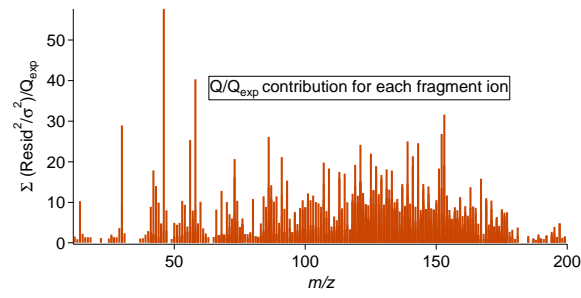
193



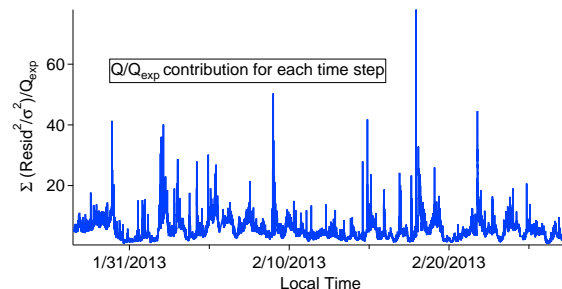
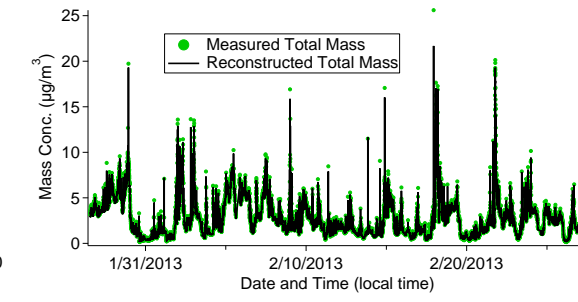
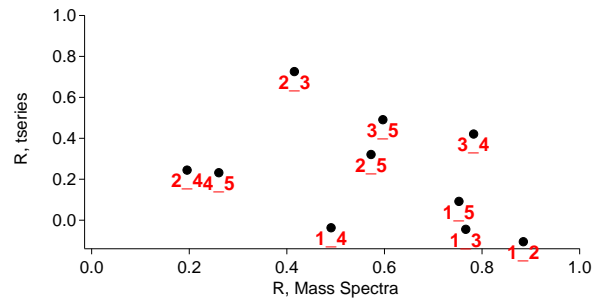
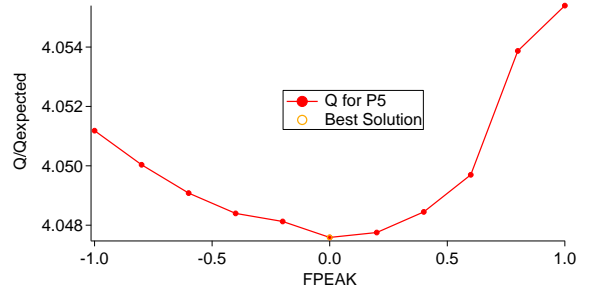
194



195



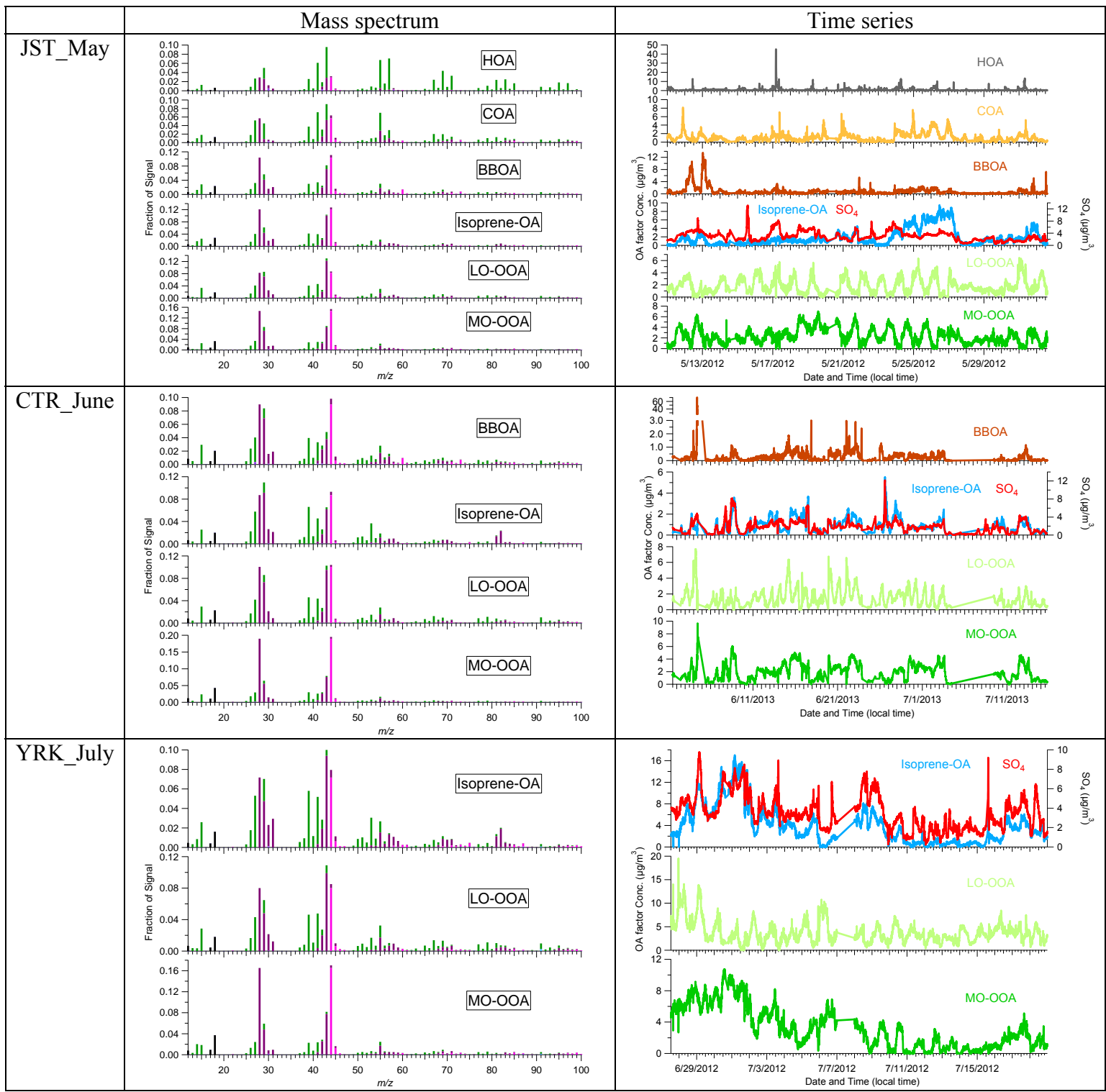
196



197

198

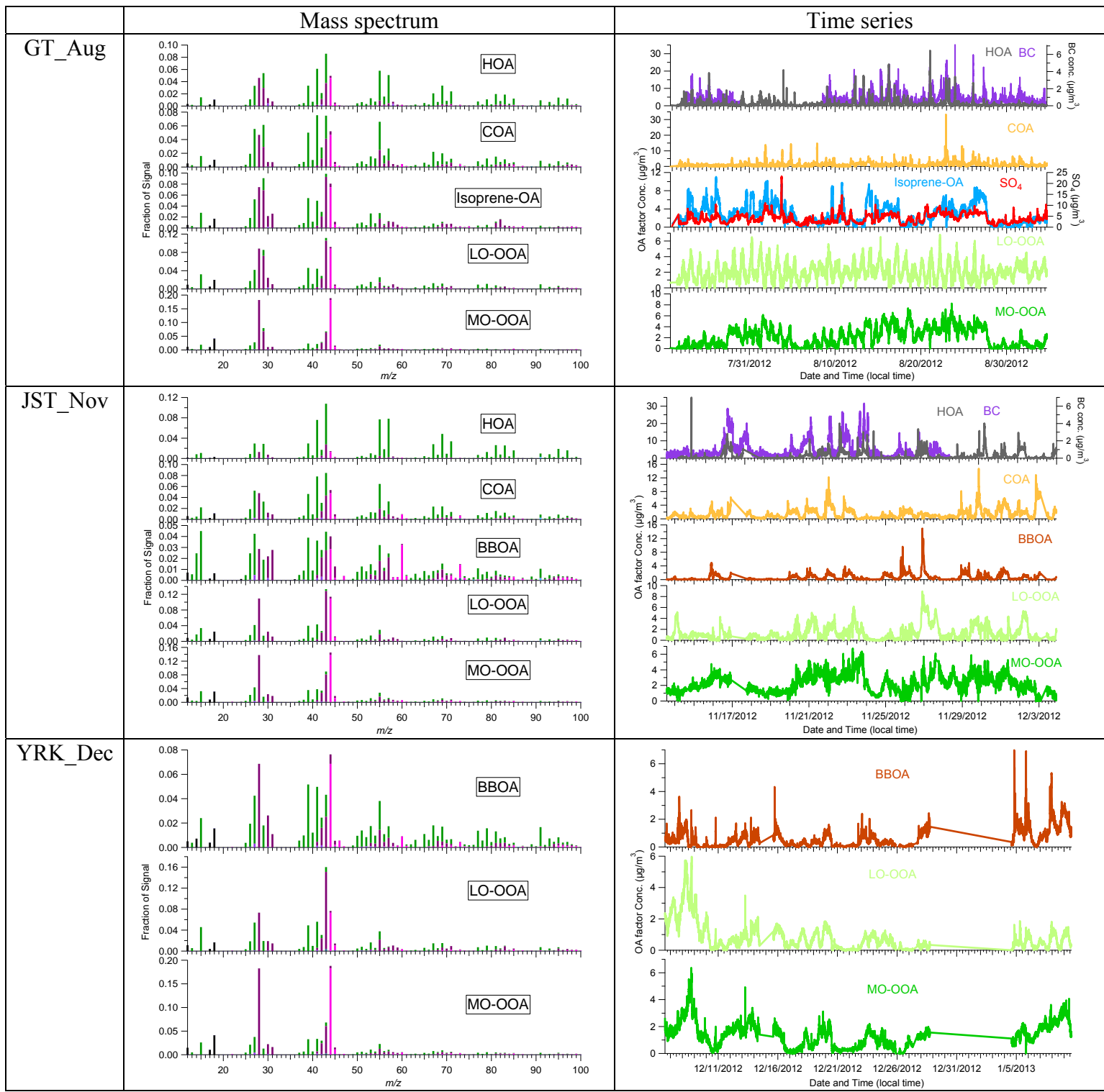
199 Fig. S2.



200

201

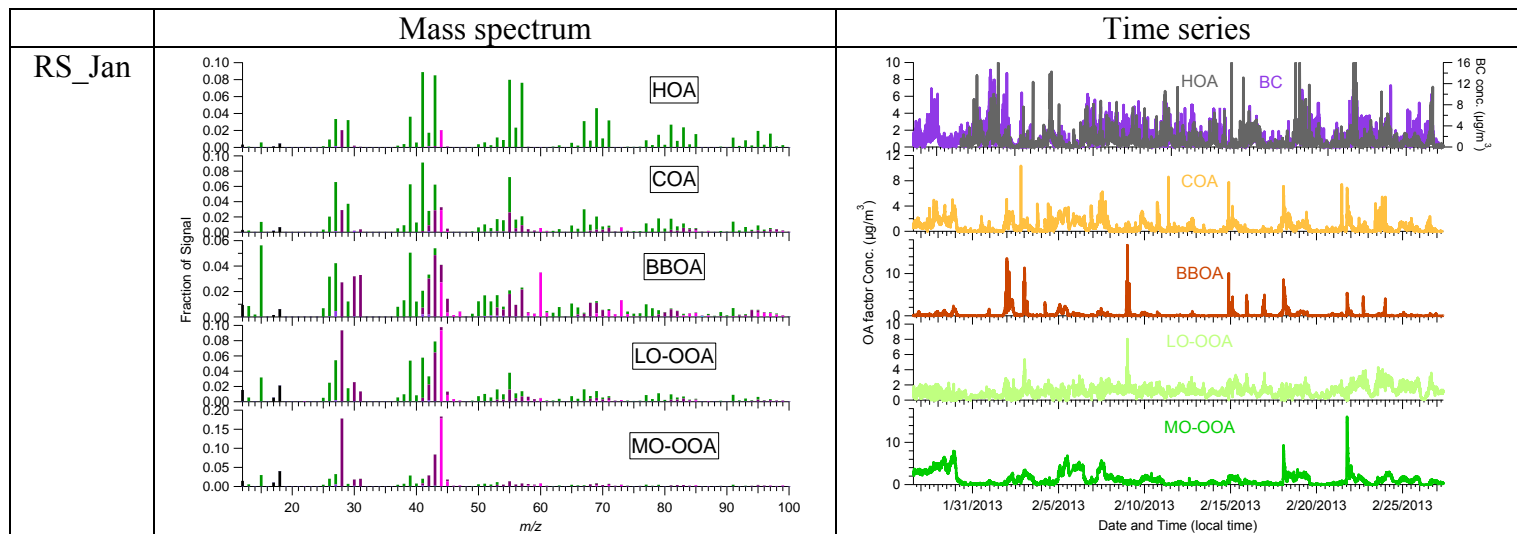
202 Fig. S2. Continued



203

204

205 Fig. S2. Continued



206

207

208

209

210

211

212

213

214

215

216

217

218

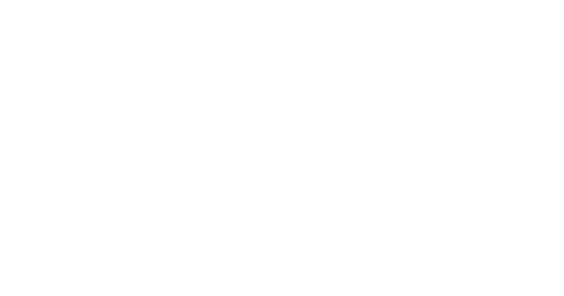
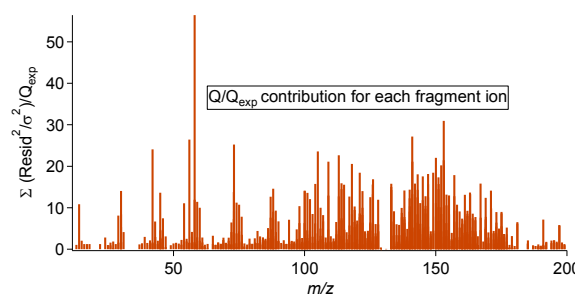
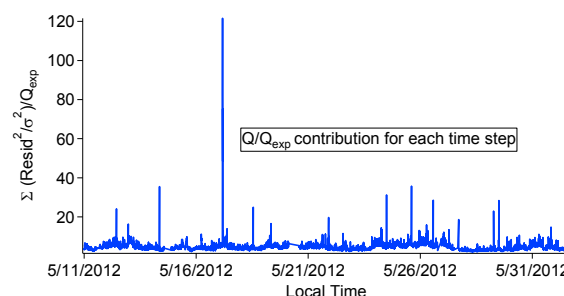
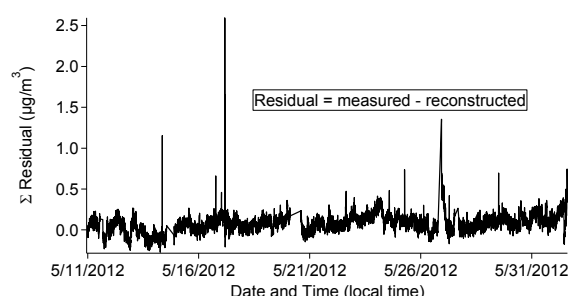
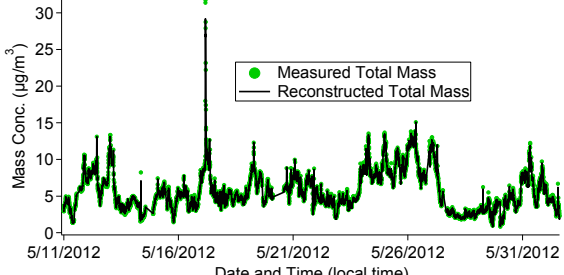
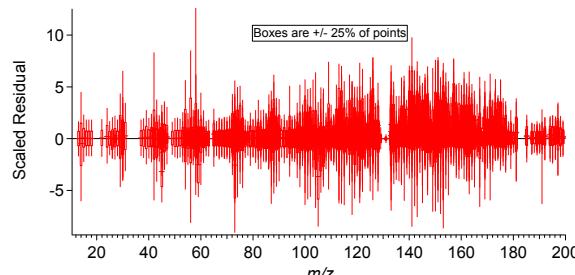
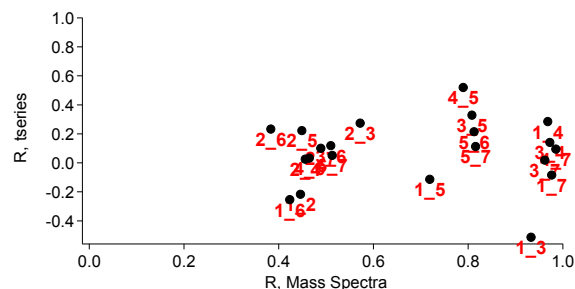
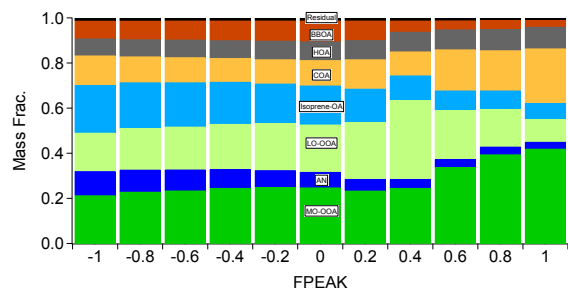
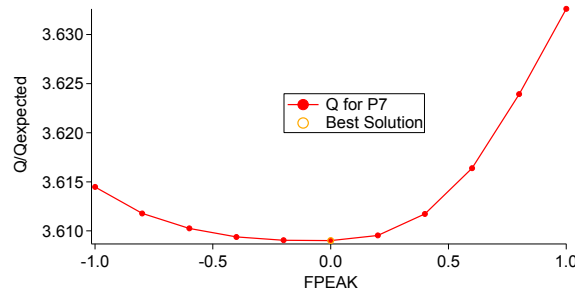
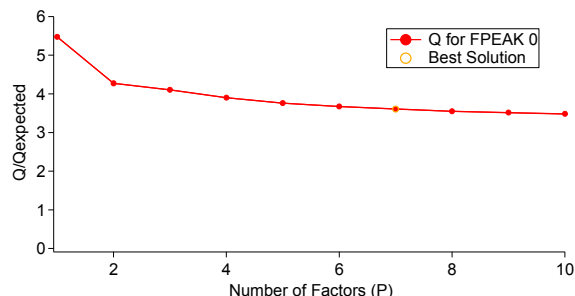
219

220

221

222 Fig. S3.

223 (a) JST\_May

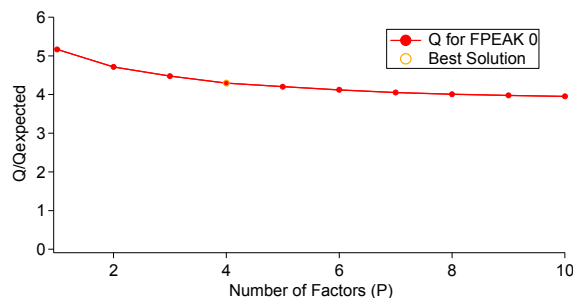


229

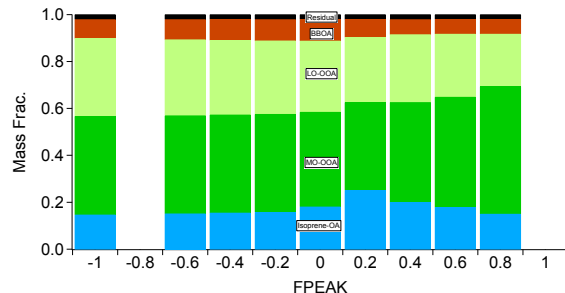
230

231

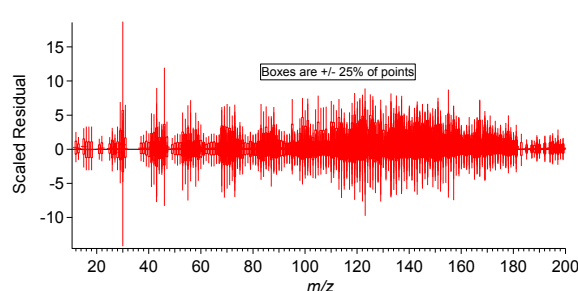
232 (b) CTR\_June



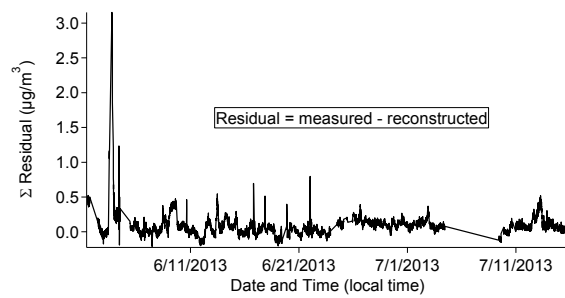
233



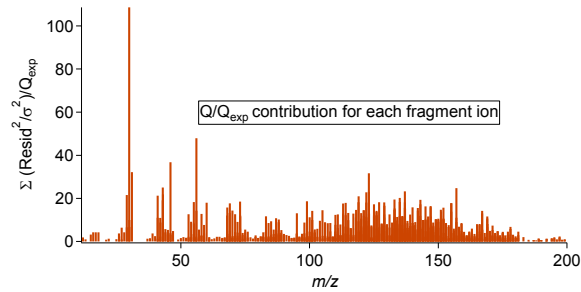
234



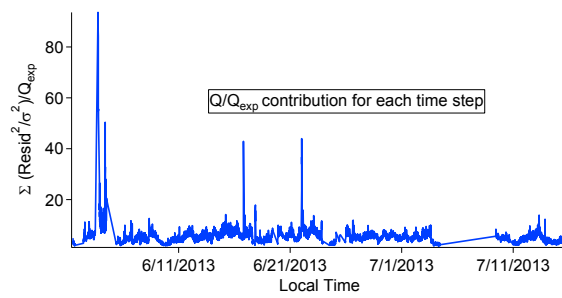
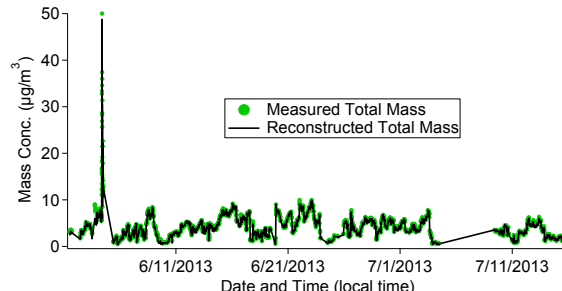
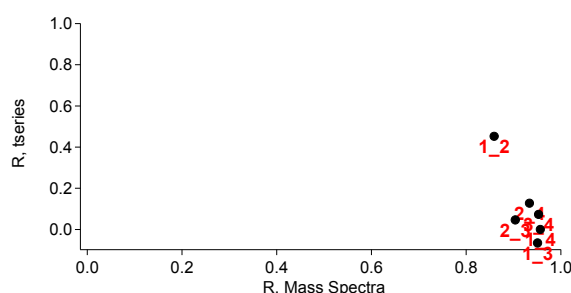
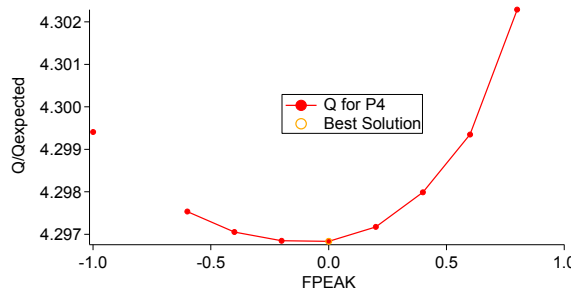
235



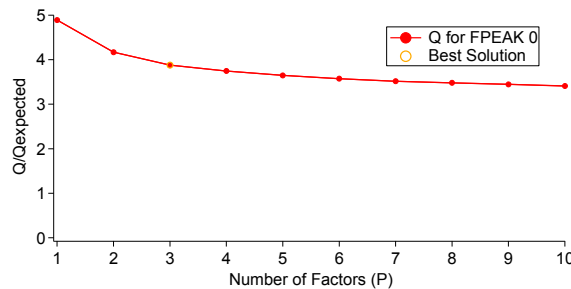
236



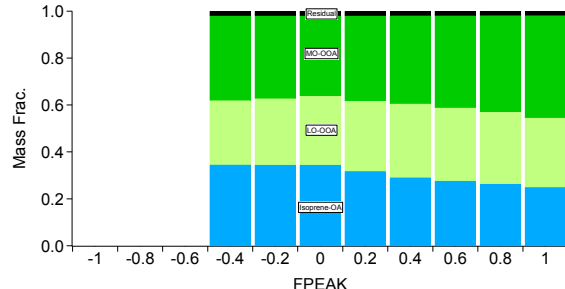
237



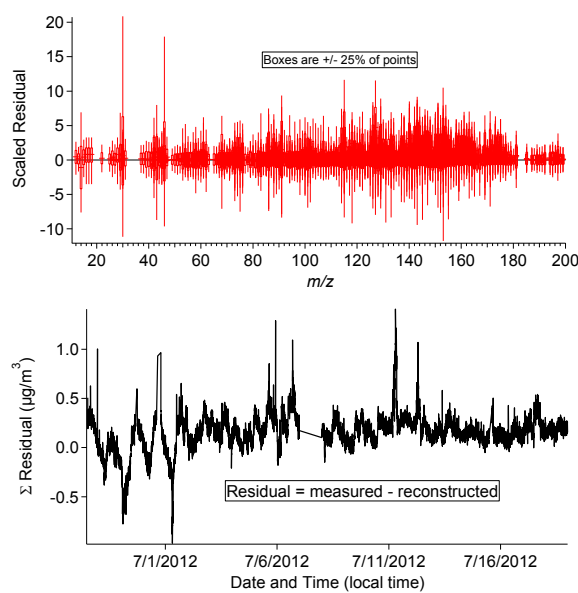
243 (c) YRK\_July



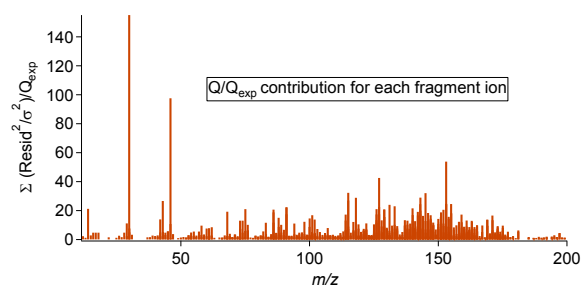
244



245



247



248

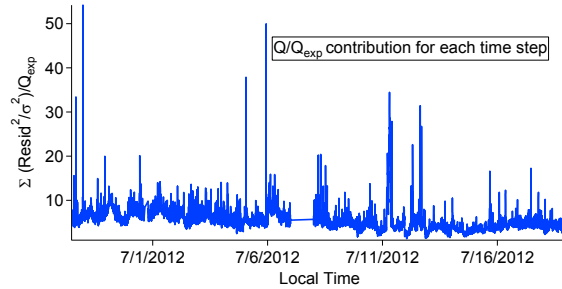
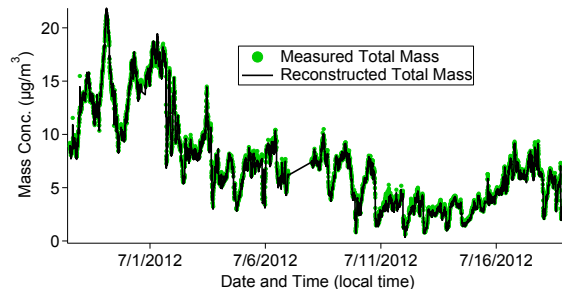
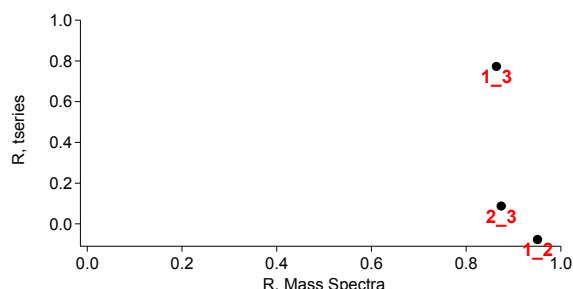
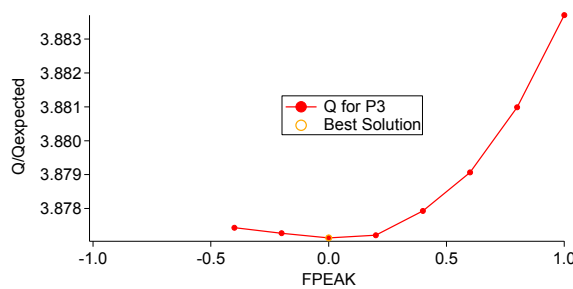
249

250

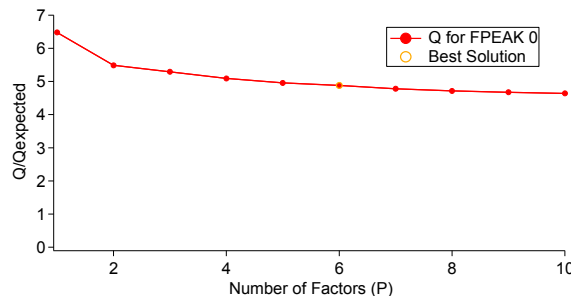
251

252

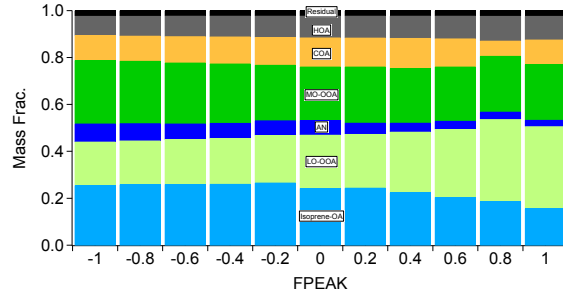
253



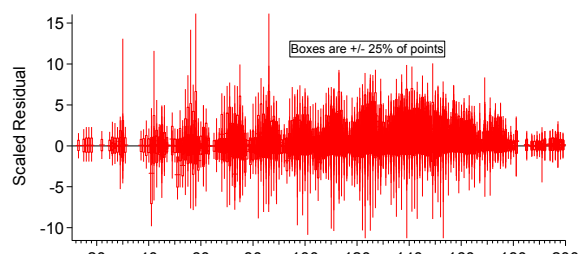
254 (d) GT\_Aug



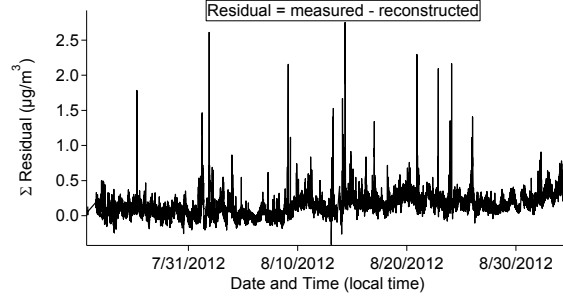
255



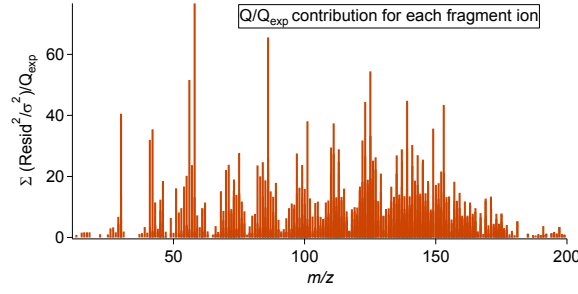
256



257



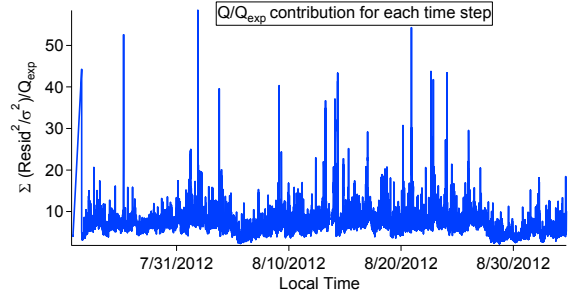
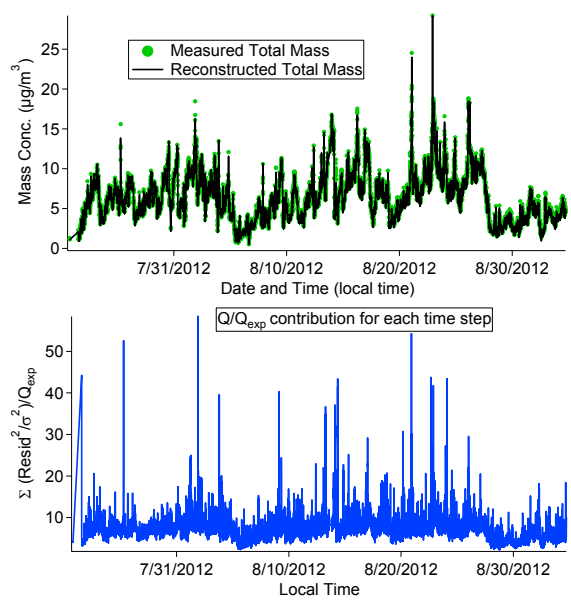
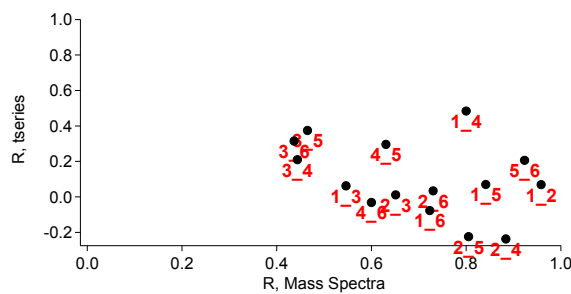
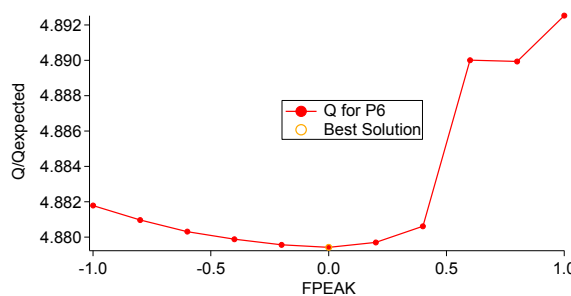
258



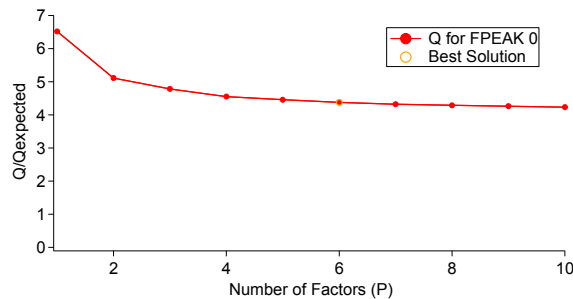
259

260

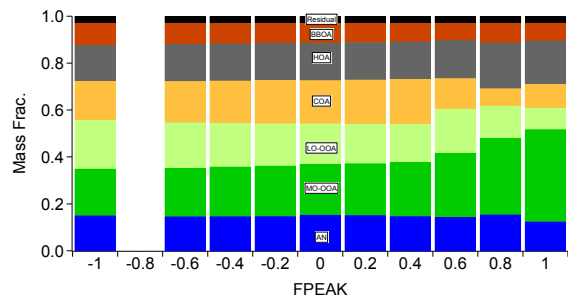
261



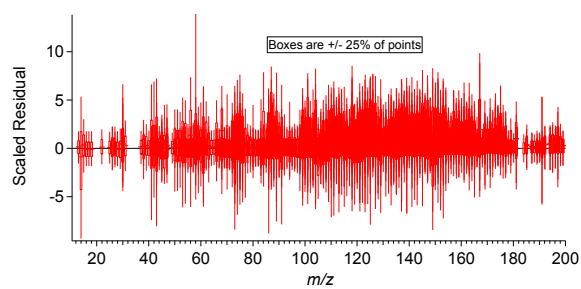
262 (e) JST\_Nov



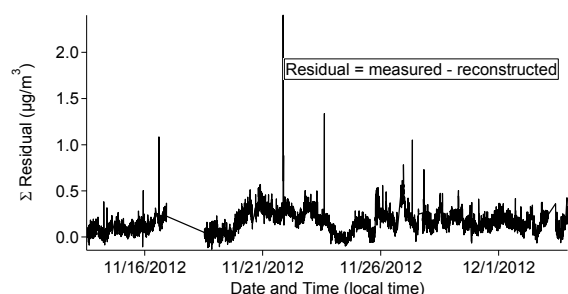
263



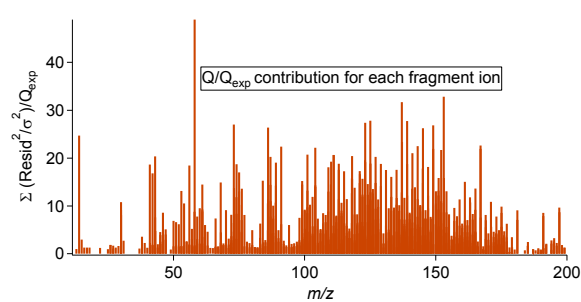
264



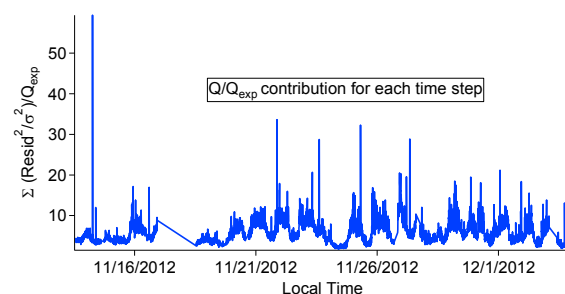
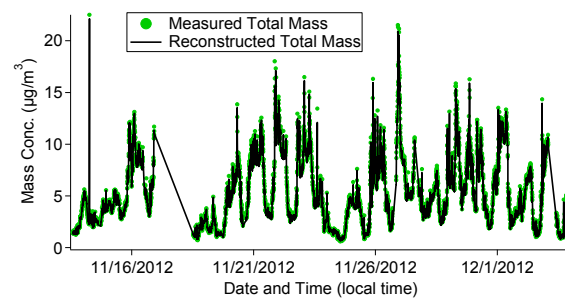
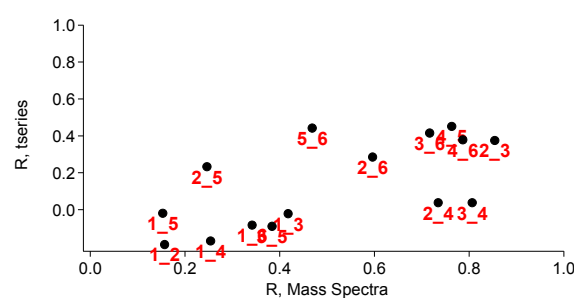
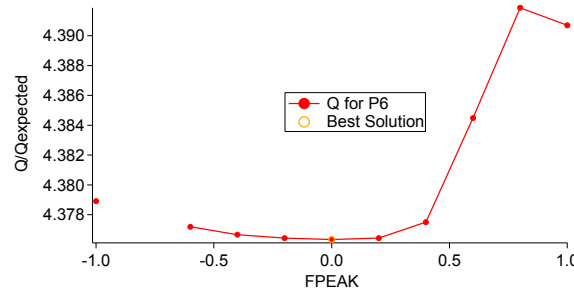
265



266



267

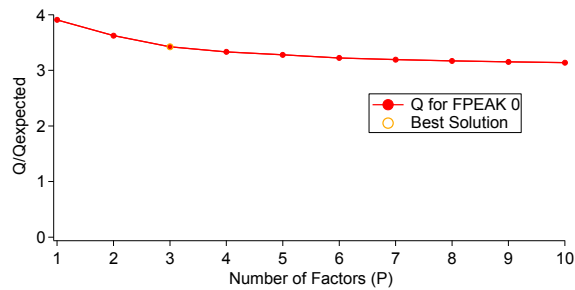


268

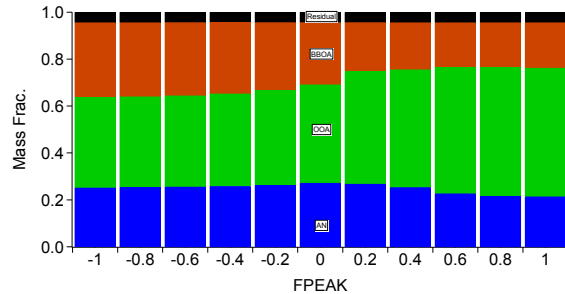
269

270

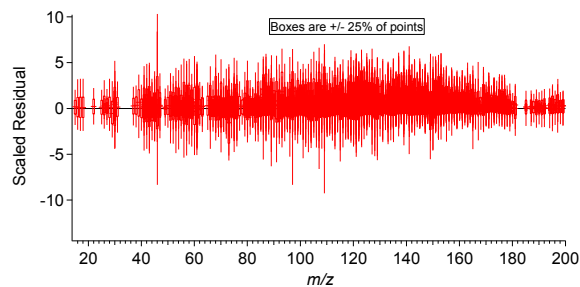
271 (f) YRK\_Dec



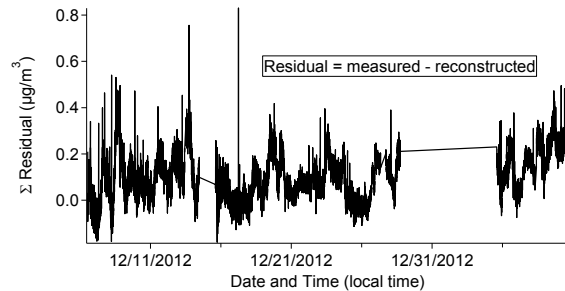
272



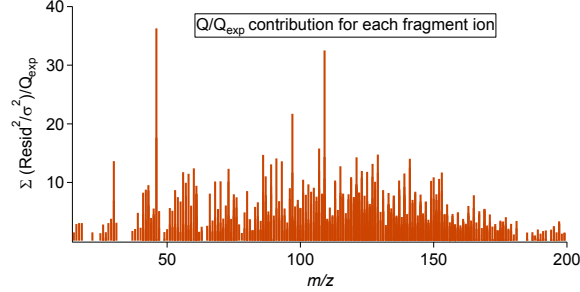
273



274



275

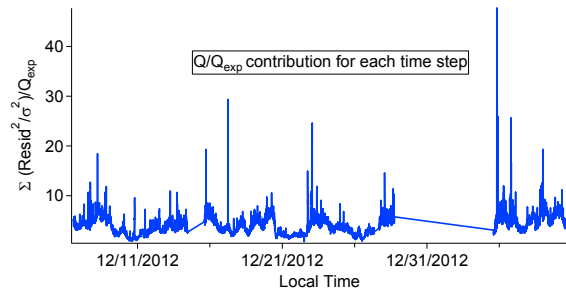
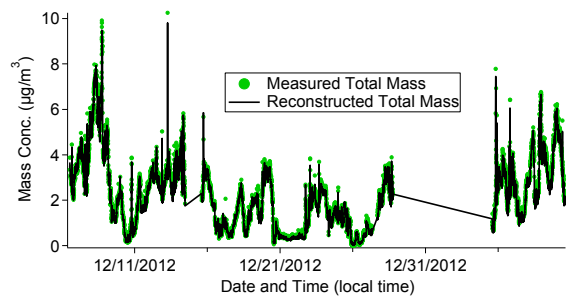
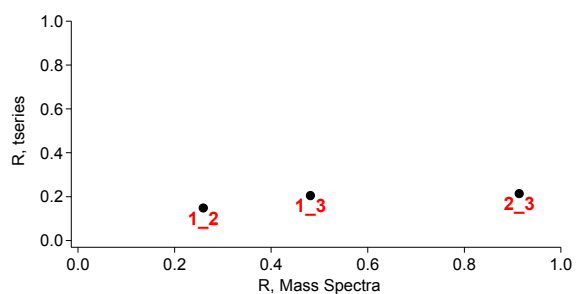
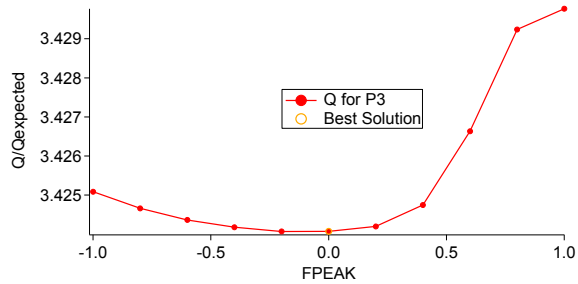


276

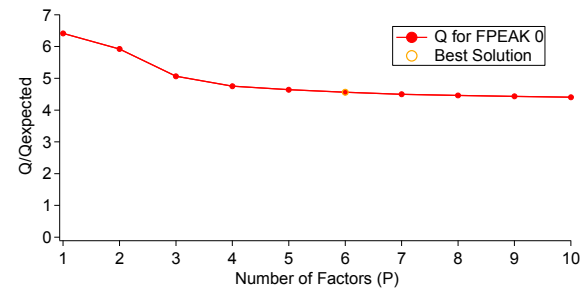
277

278

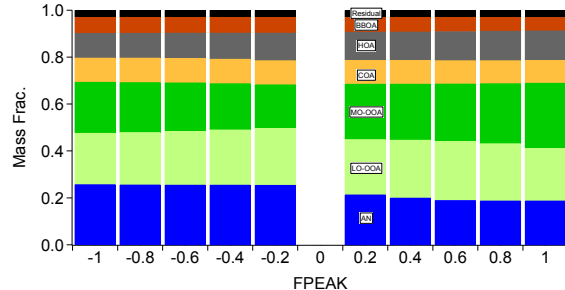
279



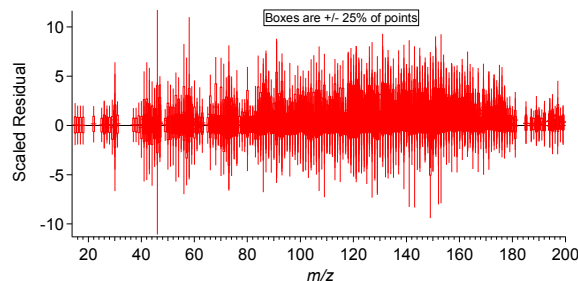
280 (g) RS\_Jan



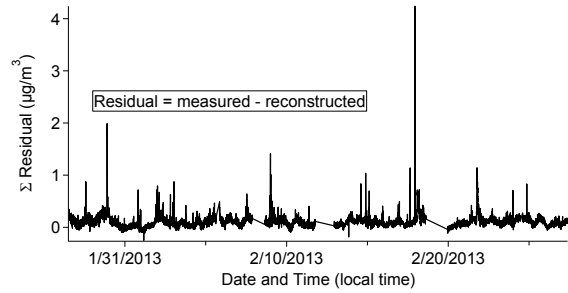
281



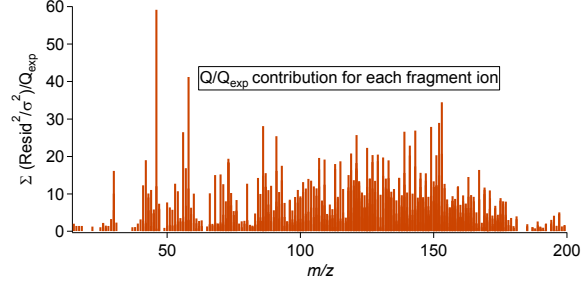
282



283



284



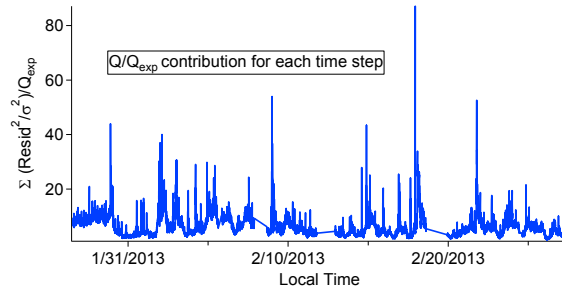
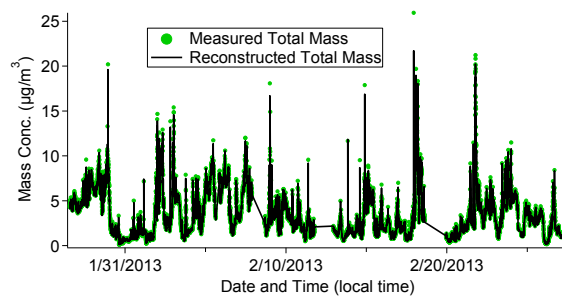
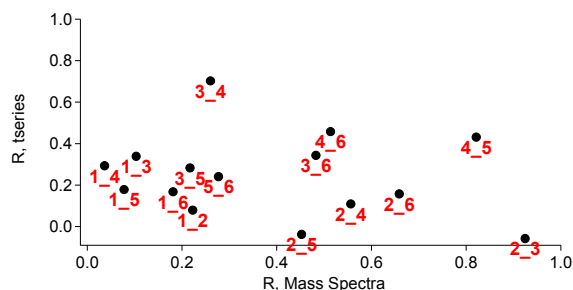
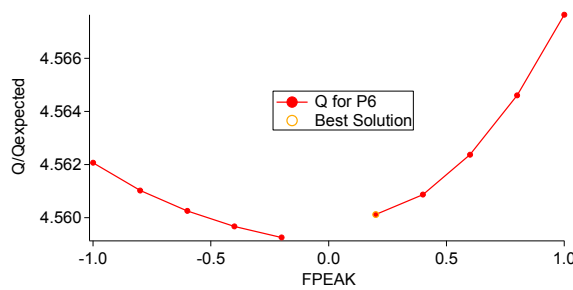
285

286

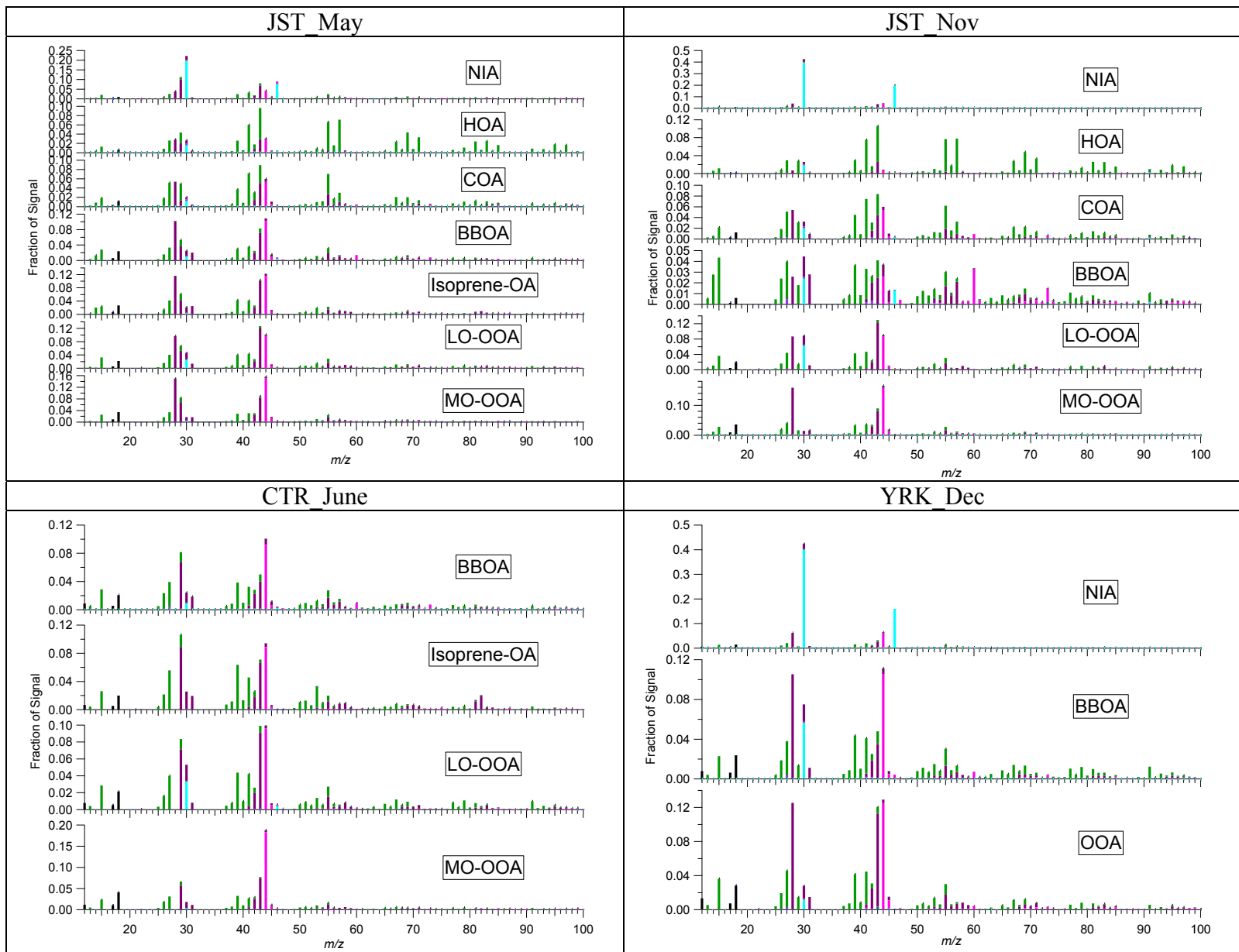
287

288

289



290 Fig. S4.



291

292

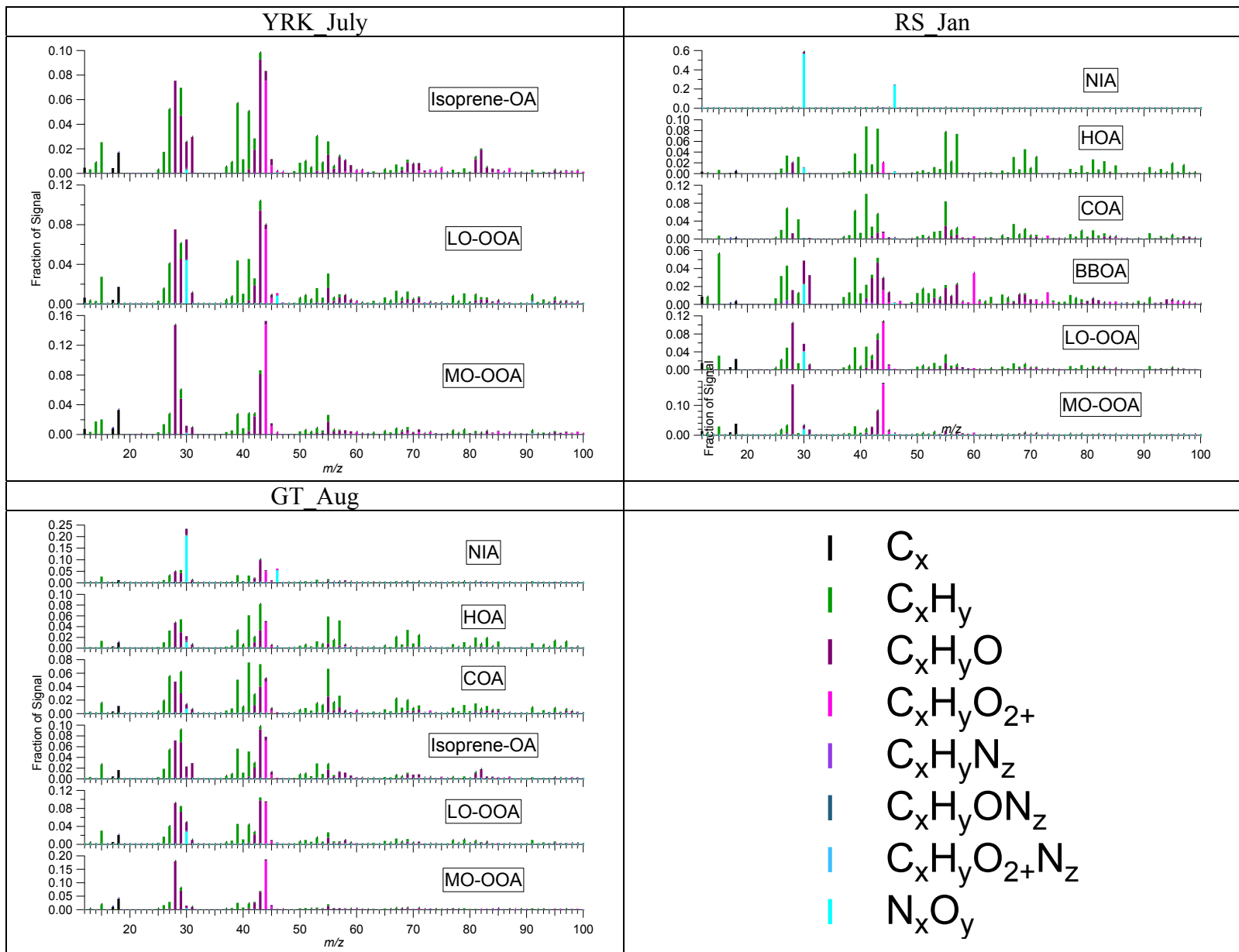
293

294

295

296

297 Fig. S4 continued



298

299

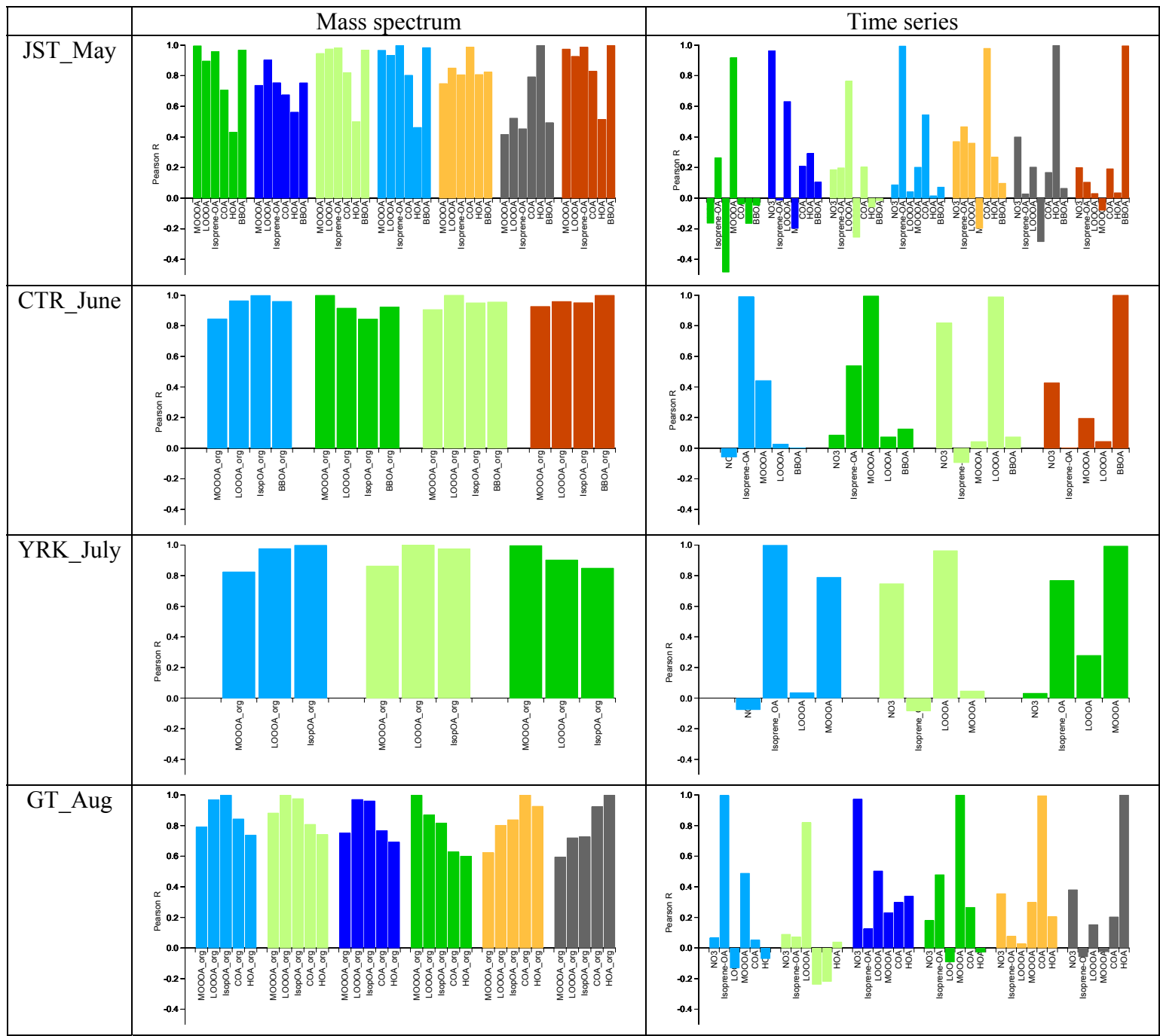
300

301

302

303

304 Fig. S5.



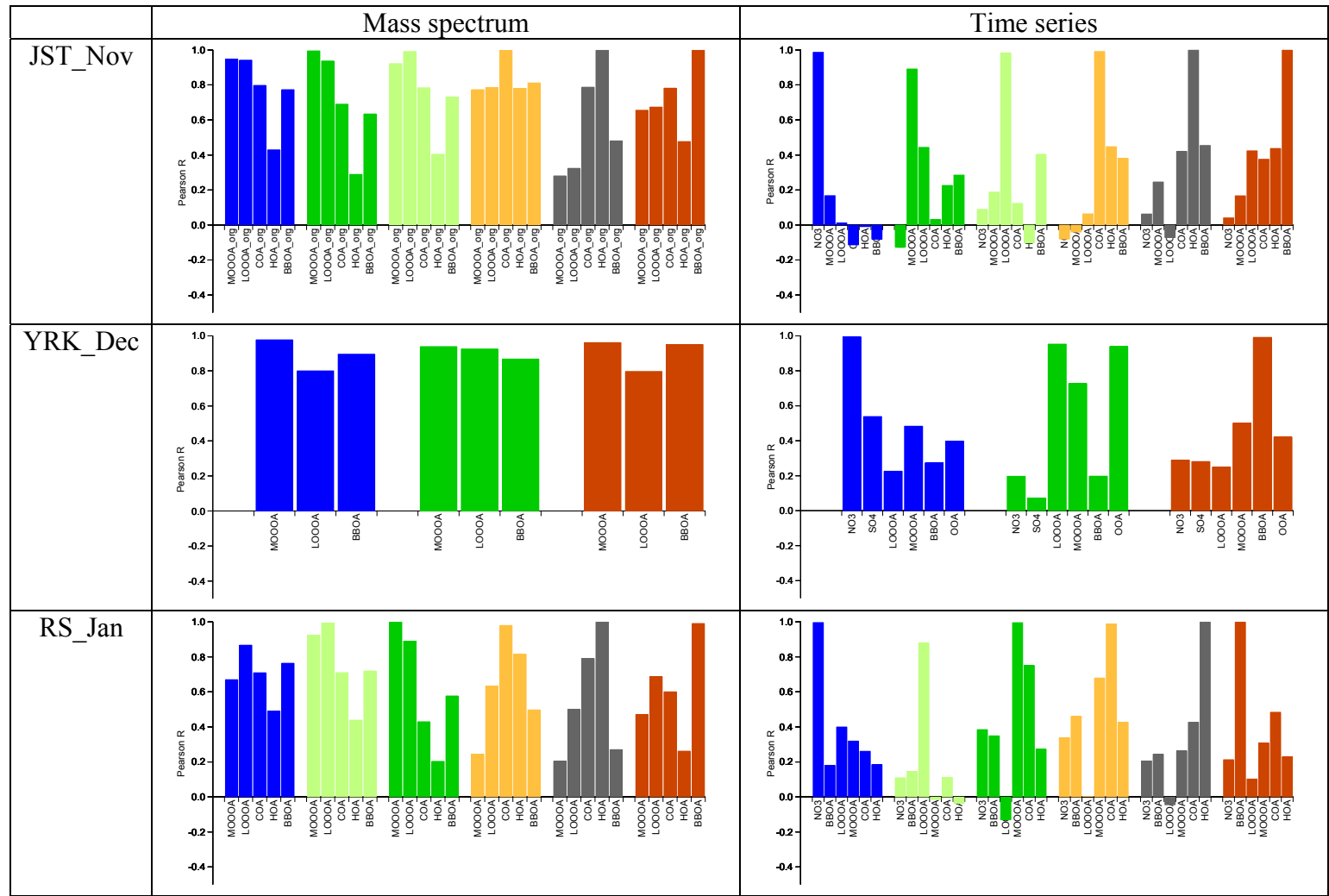
305

306

307

308

309 Fig. S5. Continued



310

311

312

313

314

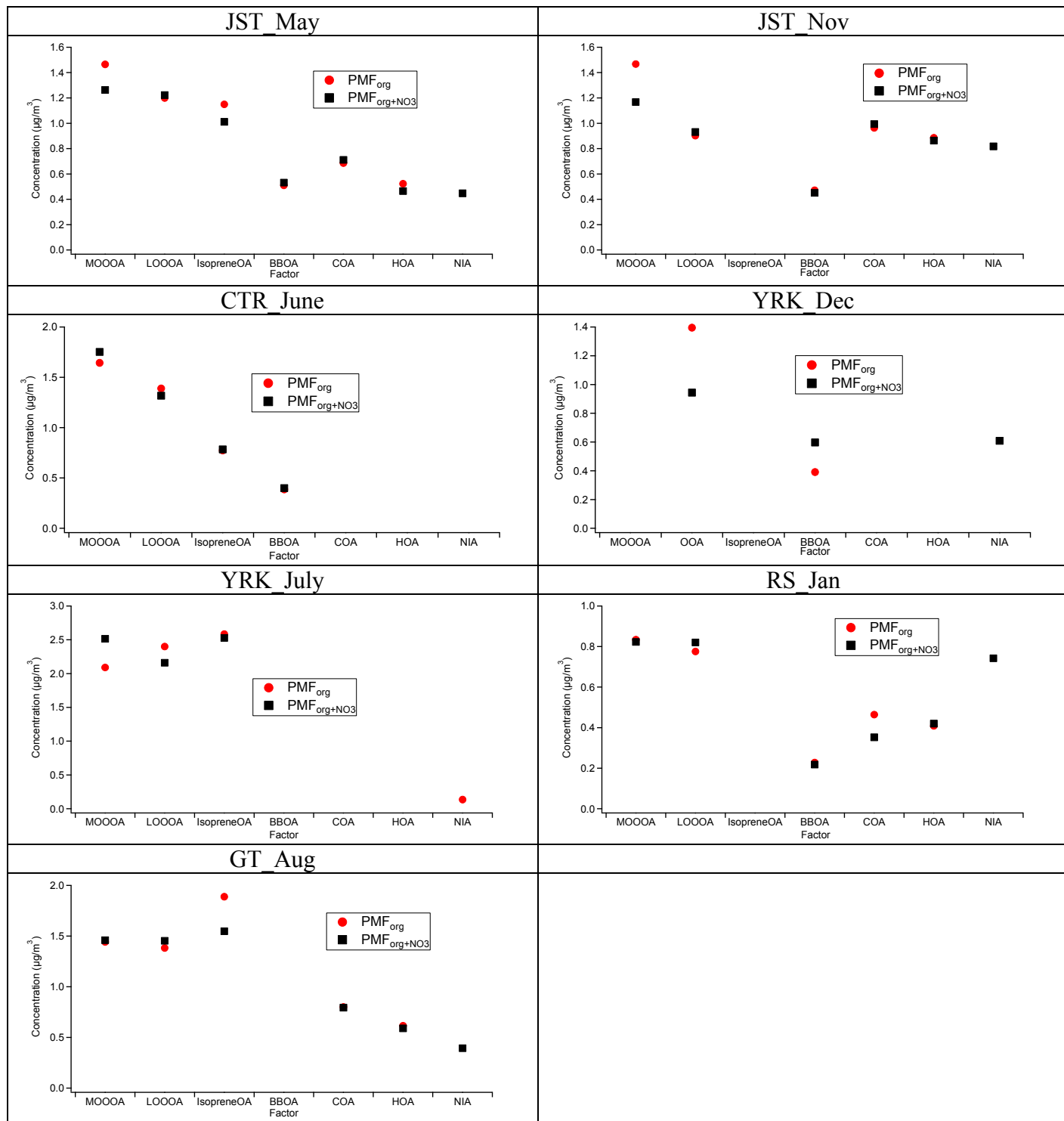
315

316

317

318

319 Fig. S6.

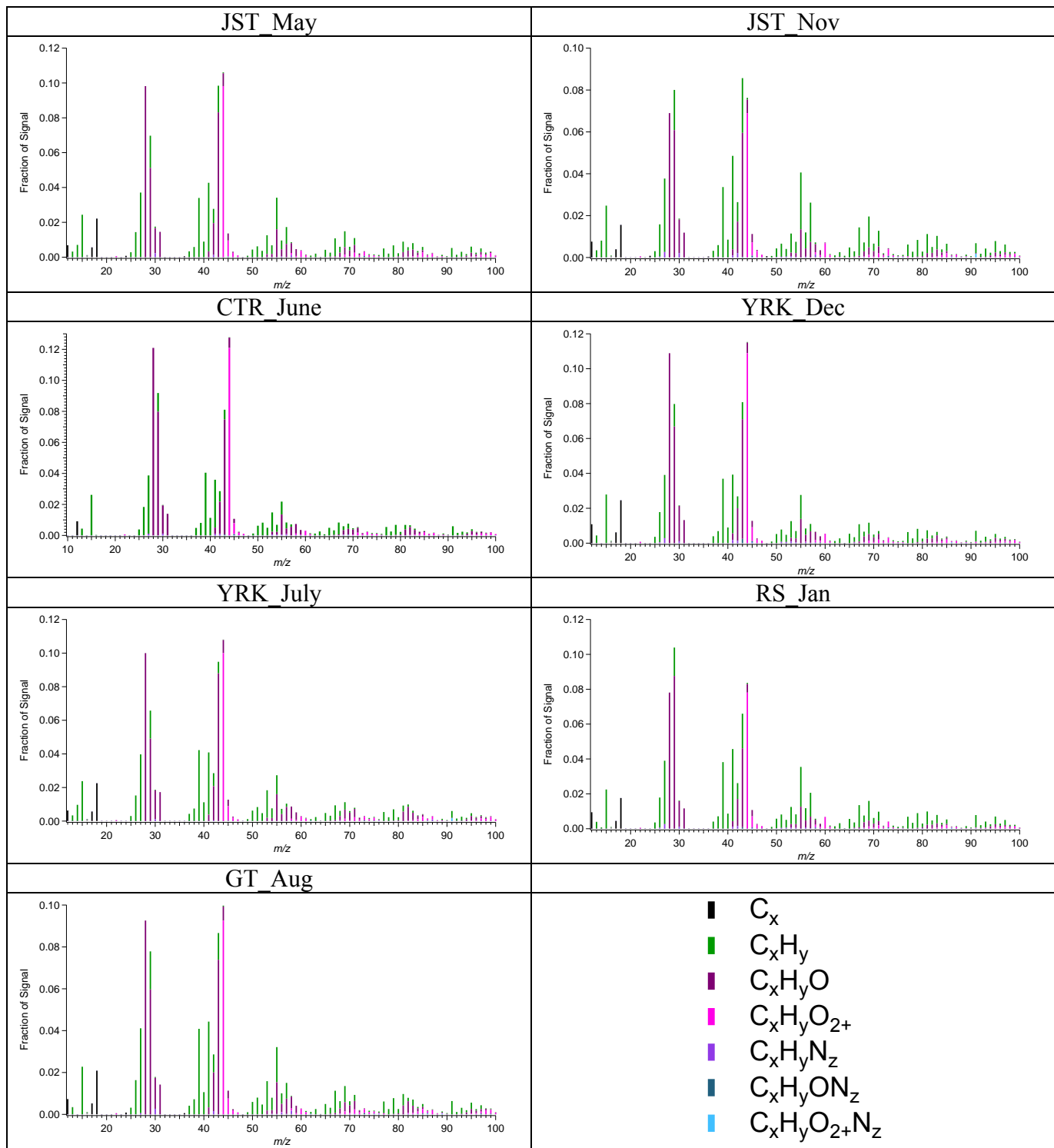


320

321

322

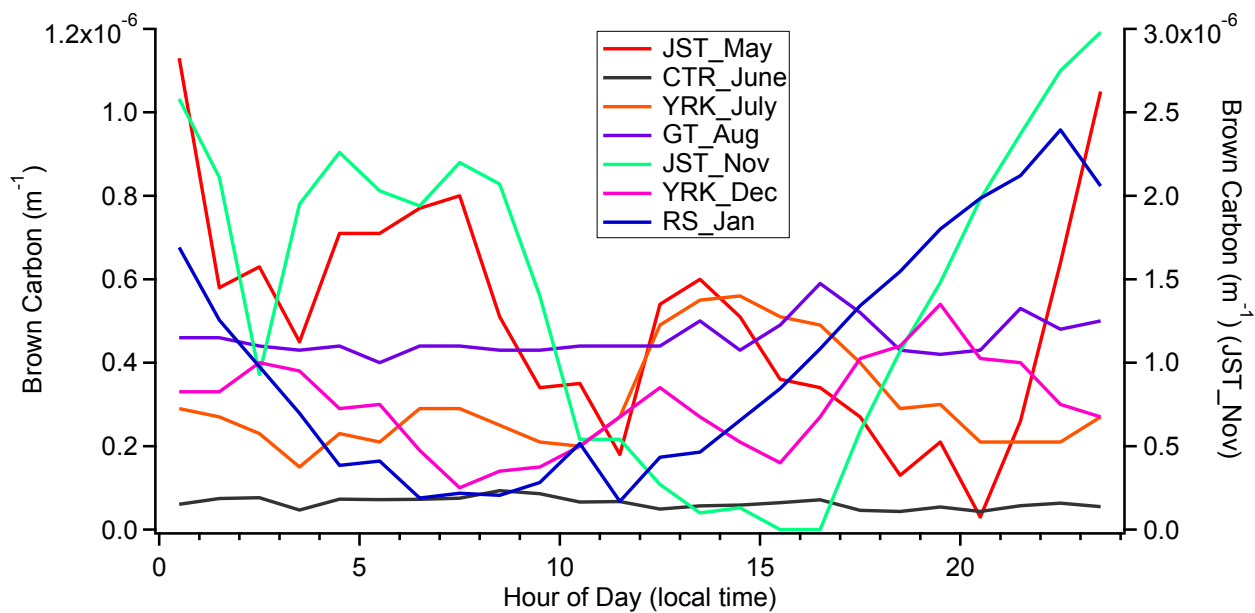
323 Fig. S7.



324

325

326 Fig. S8.



327

328

329

330

331

332

333

334

335

336

337

338

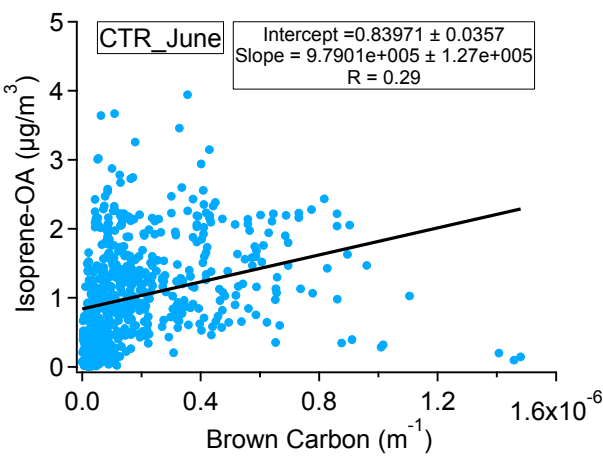
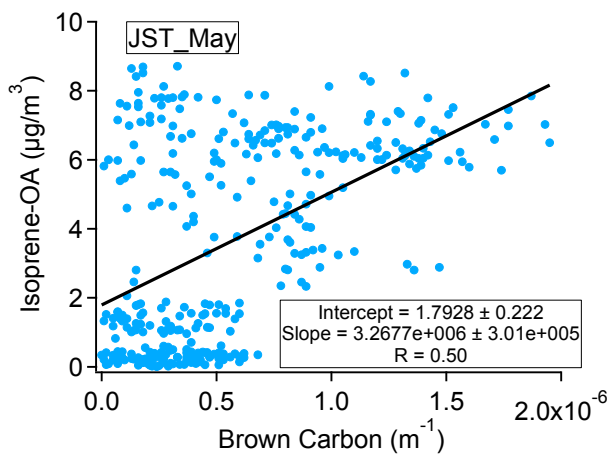
339

340

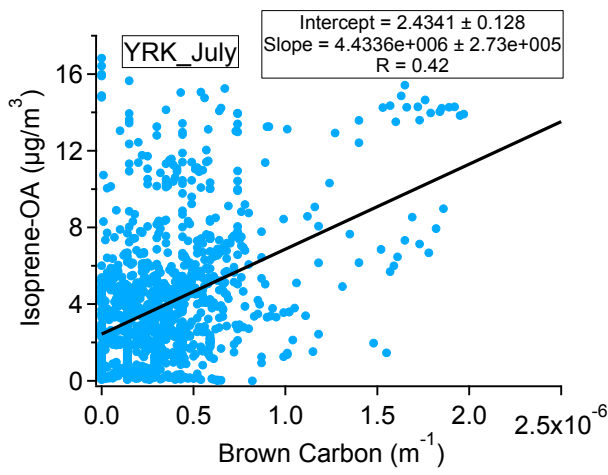
341

342

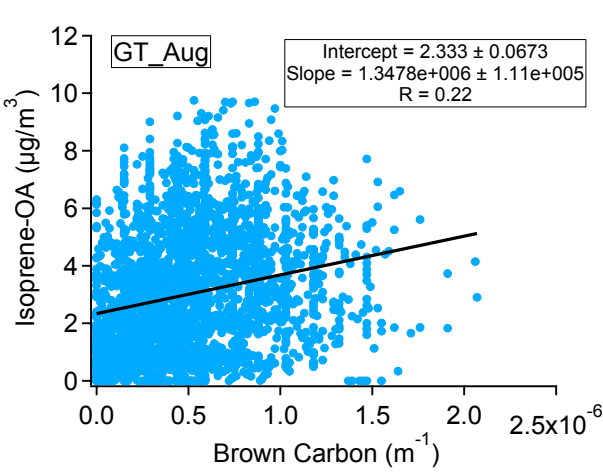
343 Fig. S9.



344



345



346

347

348

349

350

351

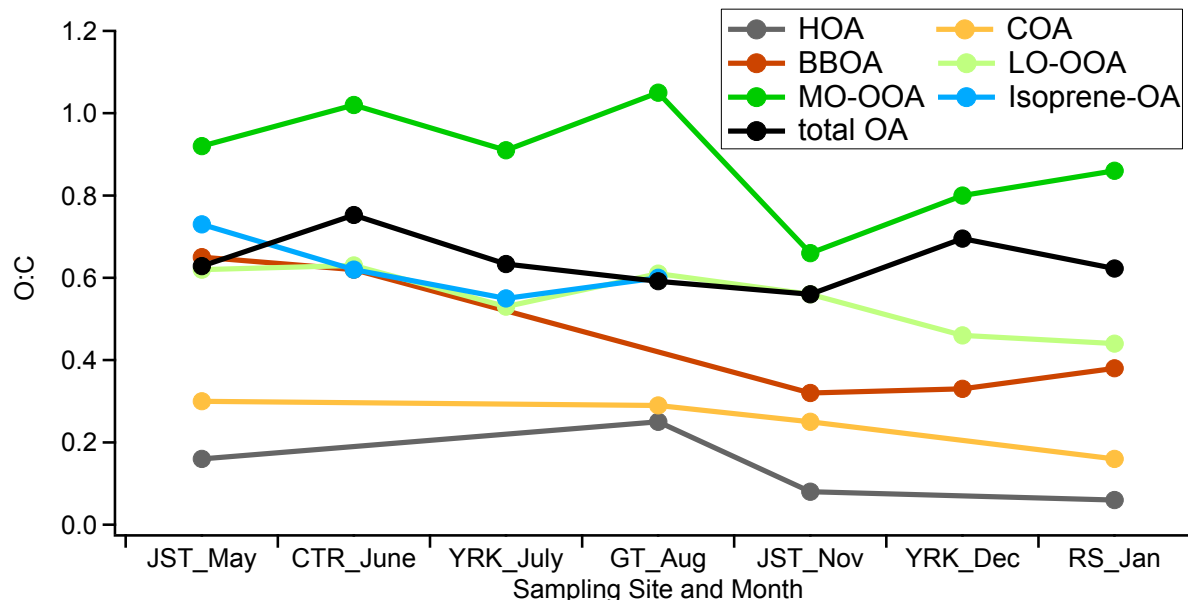
352

353

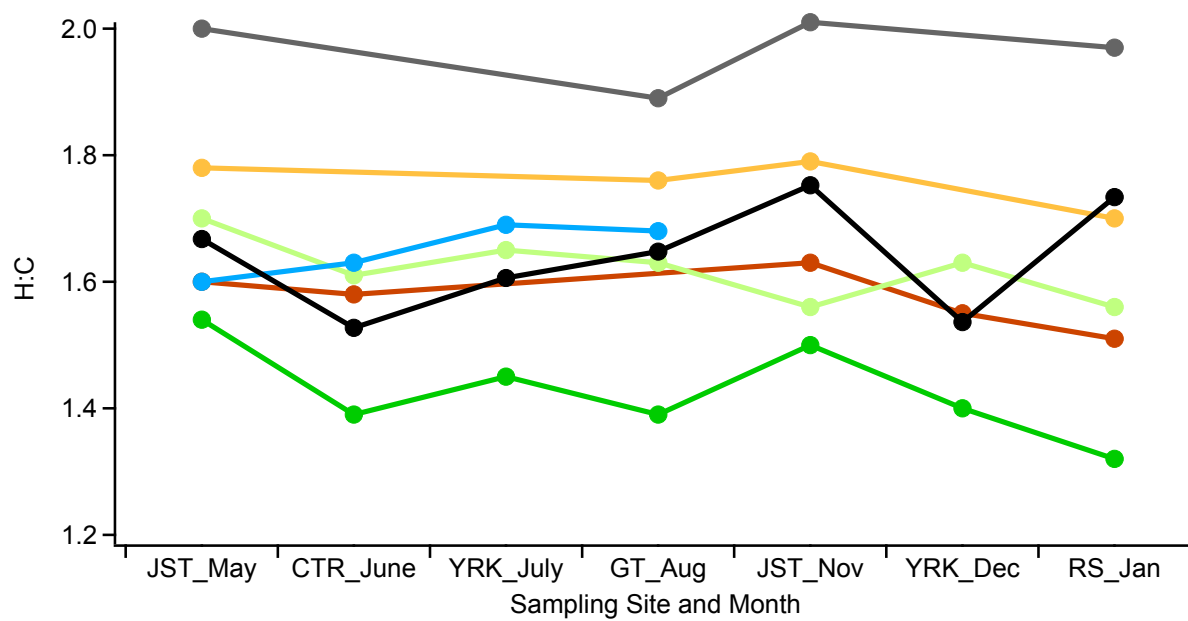
354

355

356 Fig. S10.



357



358

359

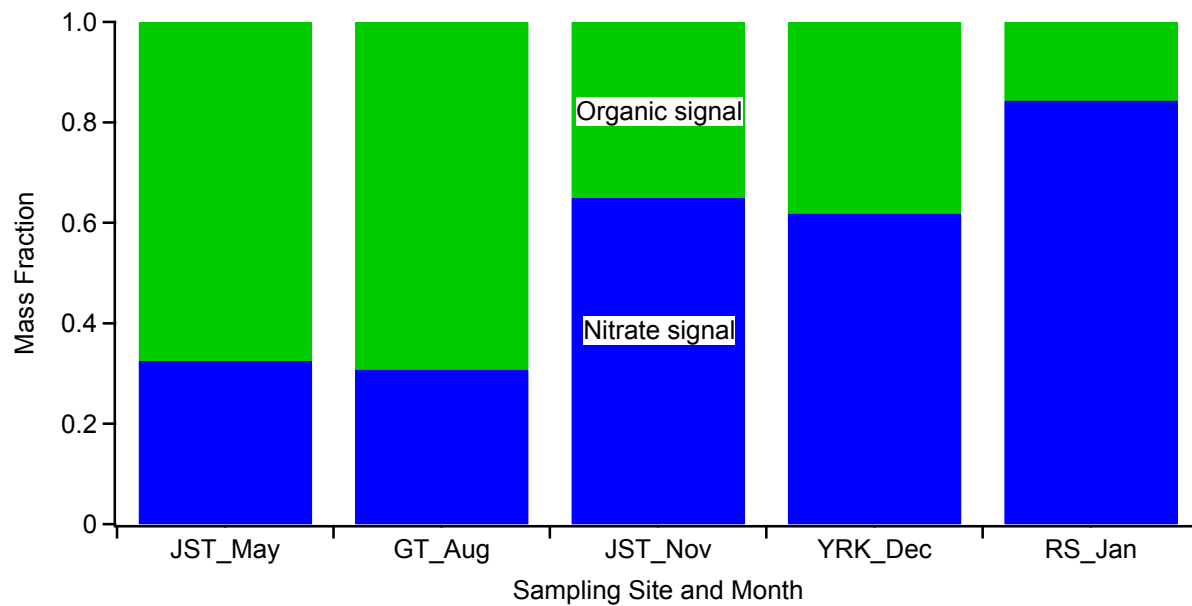
360

361

362

363

364 Fig. S11.



365

366

367

368

369

370

371

372

373

374

375

376

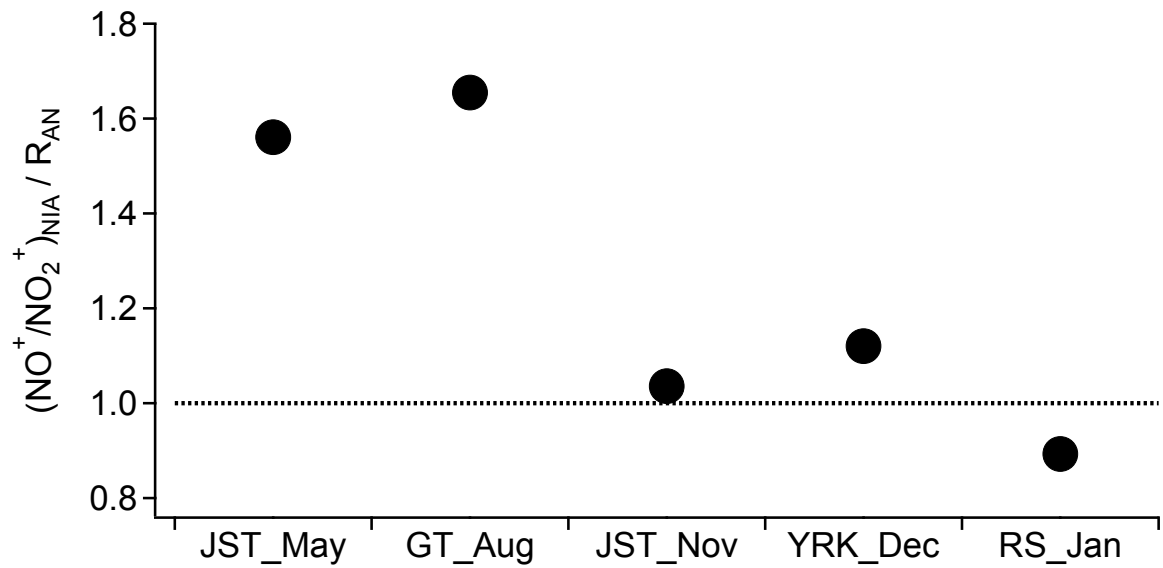
377

378

379

380

381 Fig. S12.



382

383

384

385

386

387

388

389

390

391

392

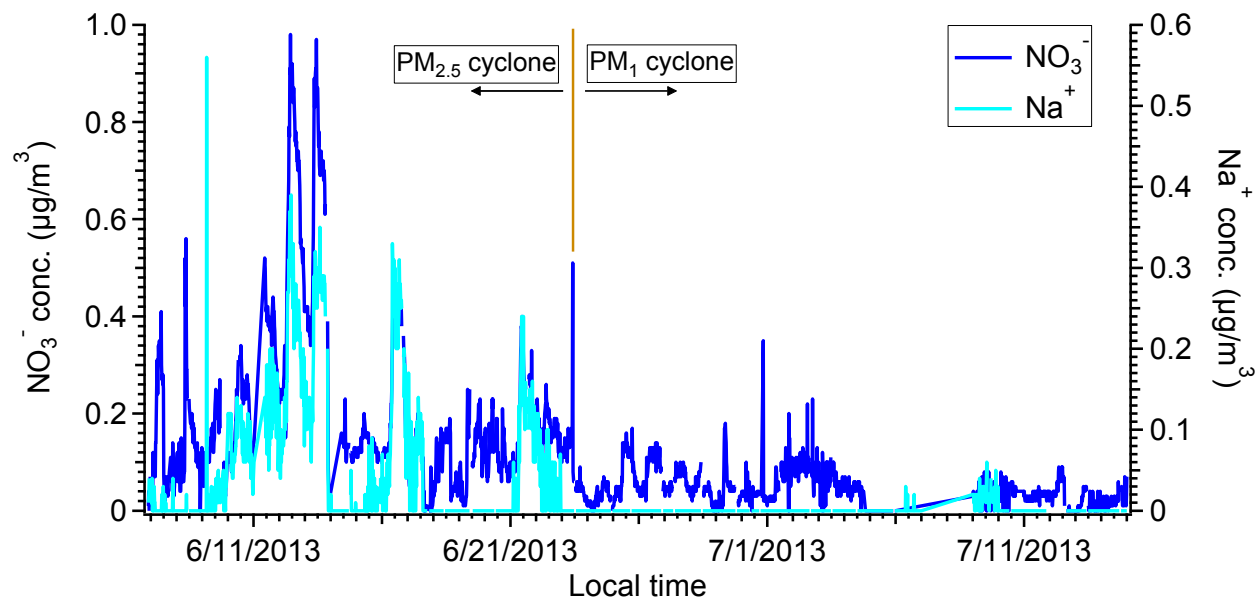
393

394

395

396

397 Fig. S13.



398

399

400

401

402

403

404

405

406

407

408

409

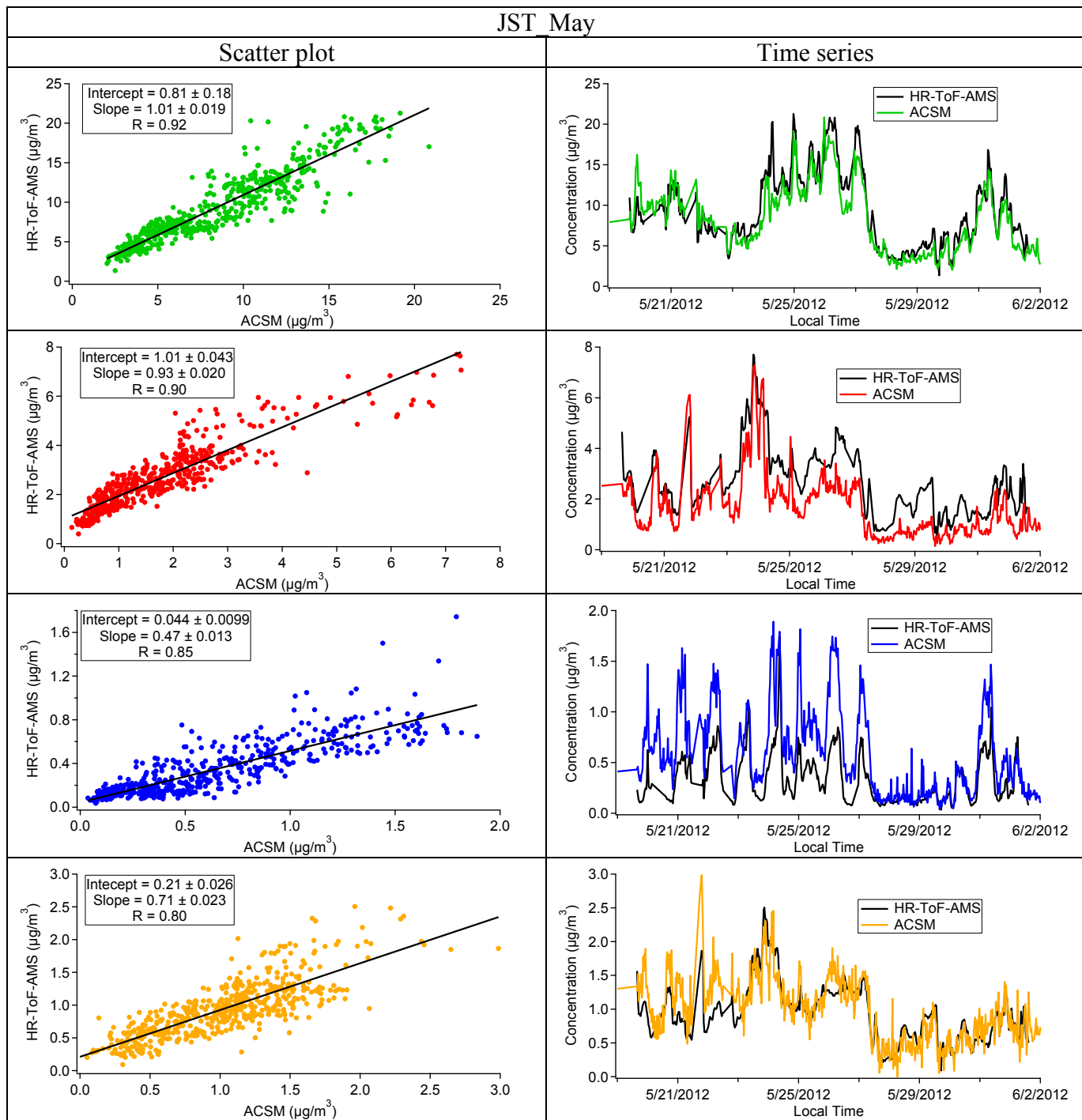
410

411

412

413

414 Fig. S14.



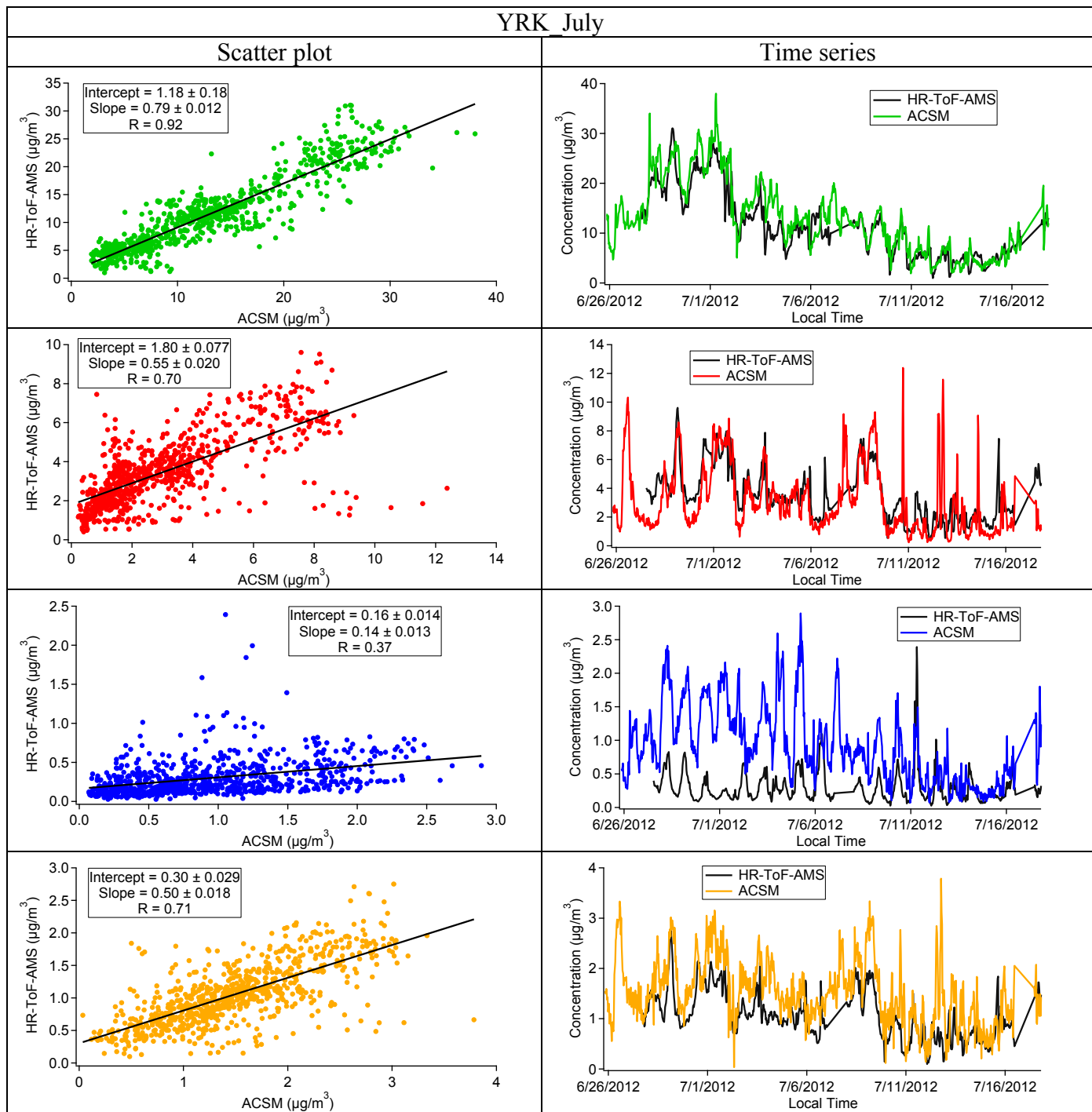
415

416

417

418

419 Fig. S14. Continued



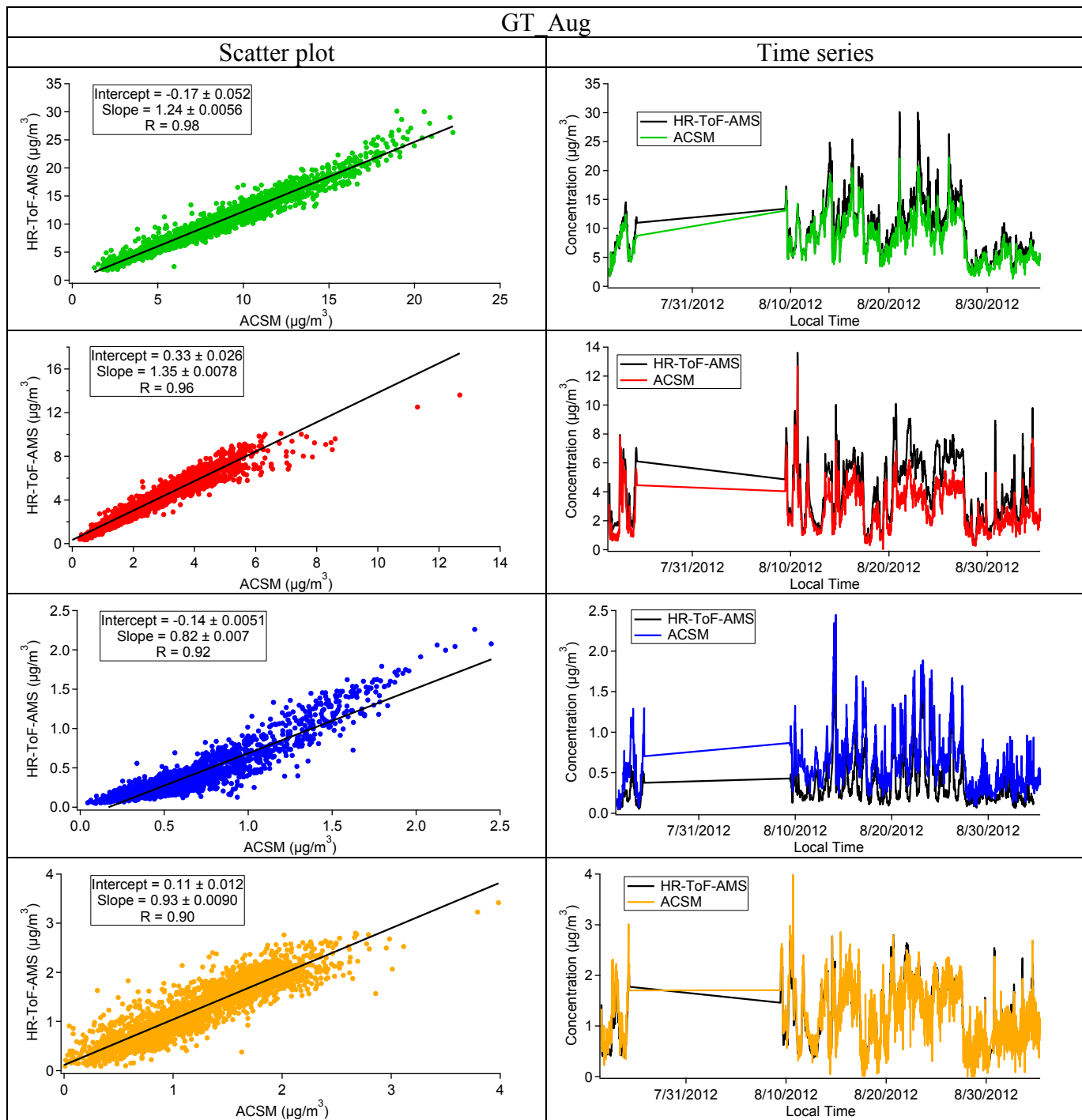
420

421

422

423

424 Fig. S14. Continued



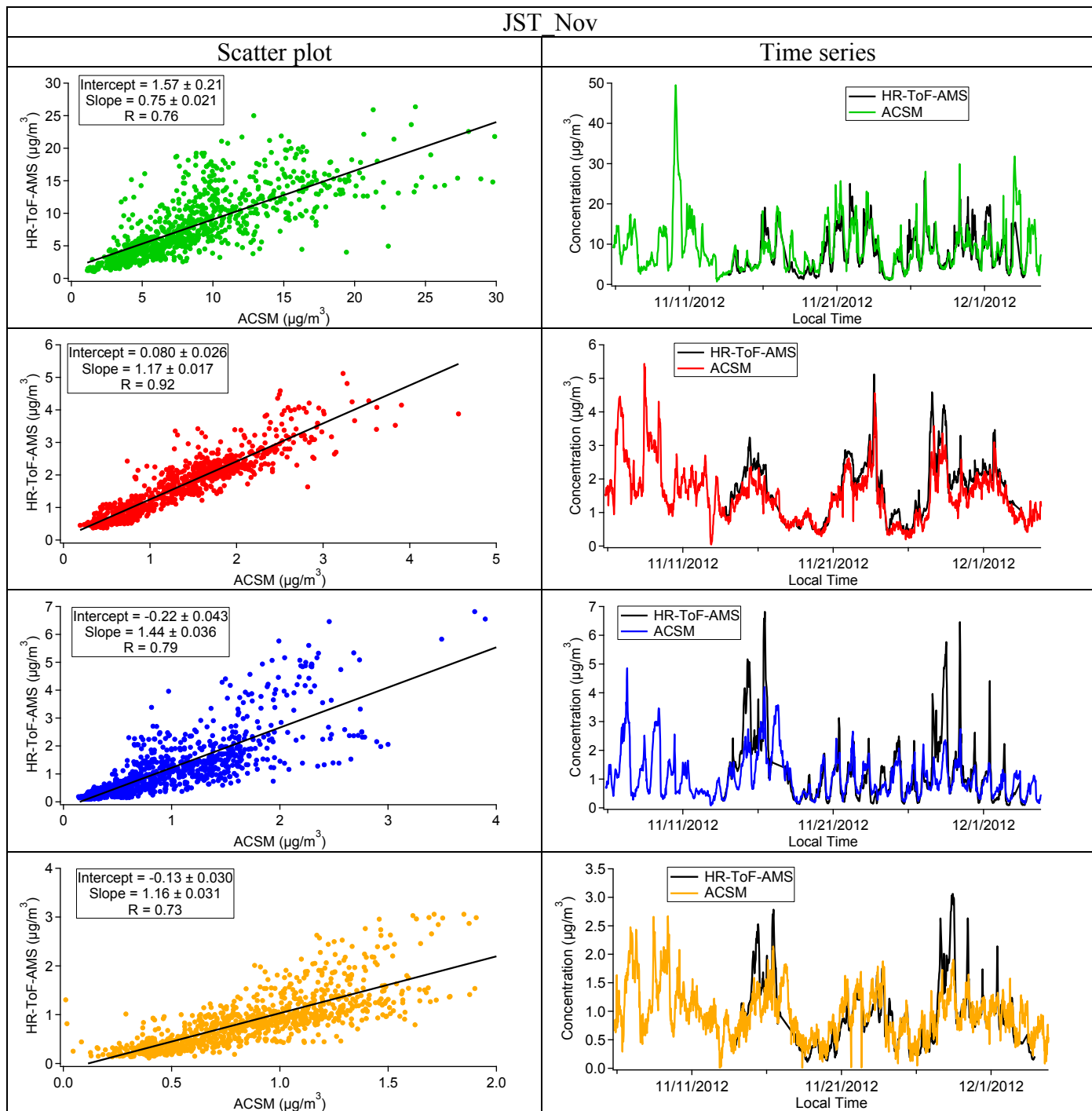
425

426

427

428

429 Fig. S14. Continued



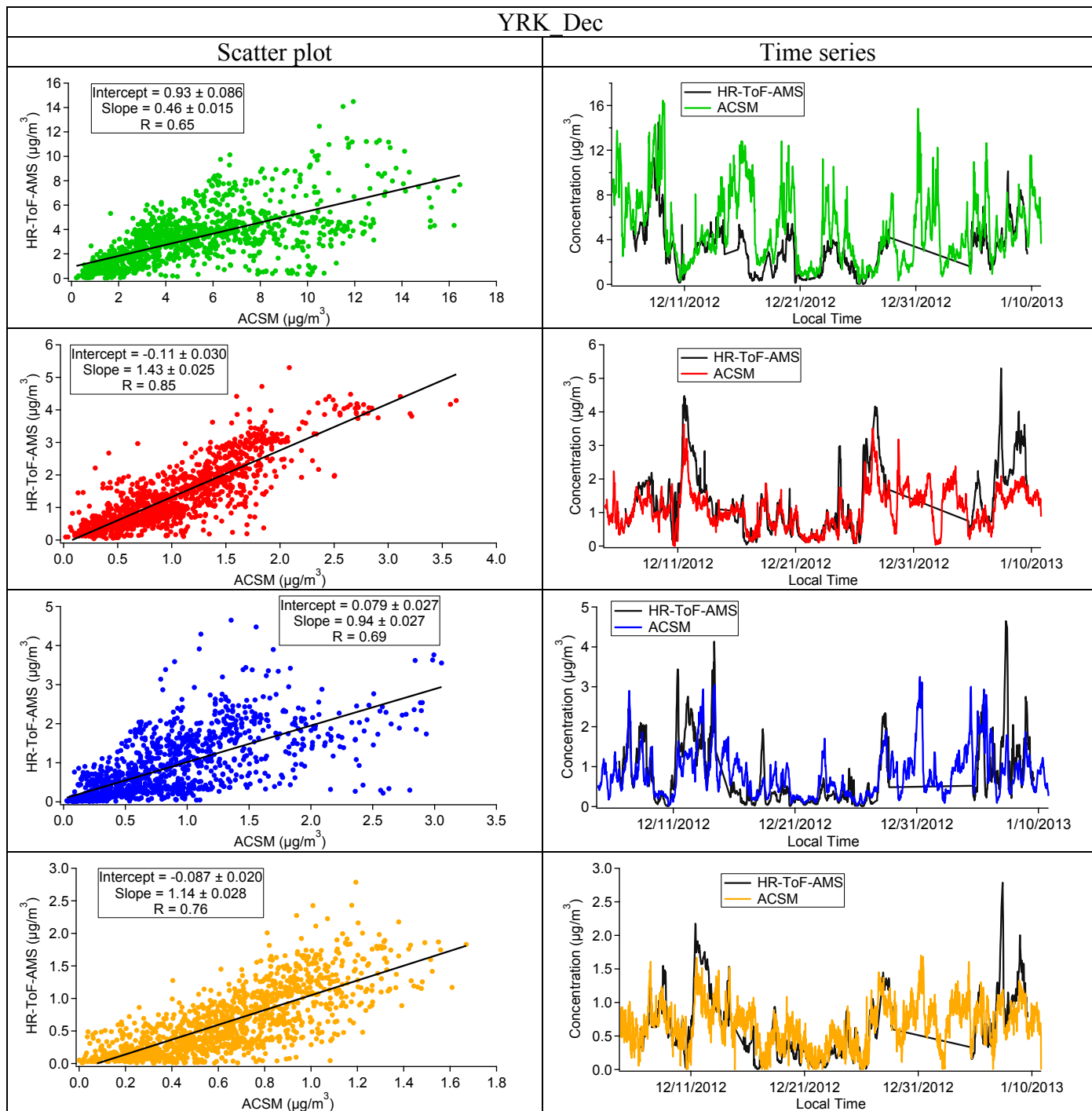
430

431

432

433

434 Fig. S14. Continued



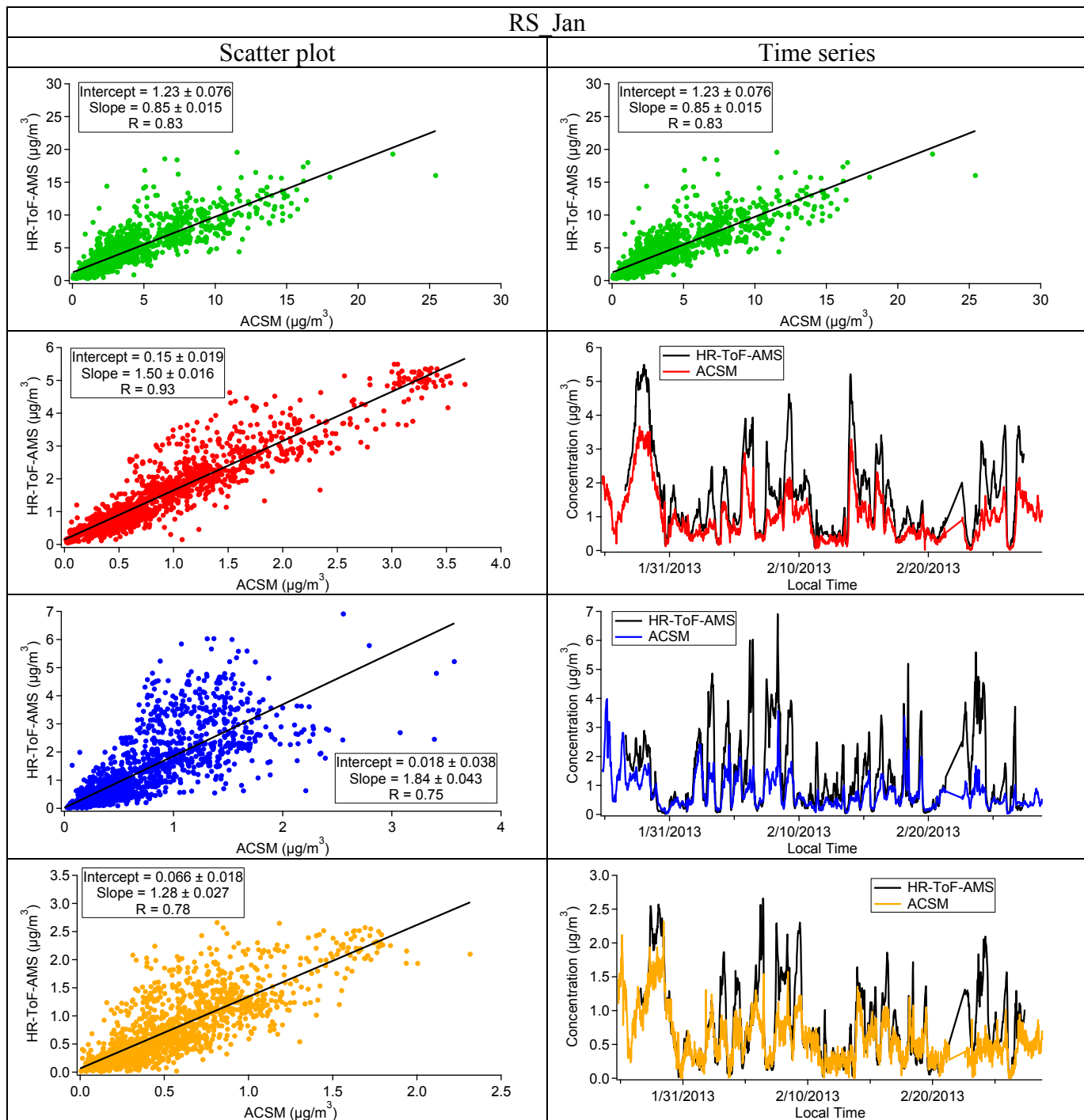
435

436

437

438

439 Fig. S14. Continued



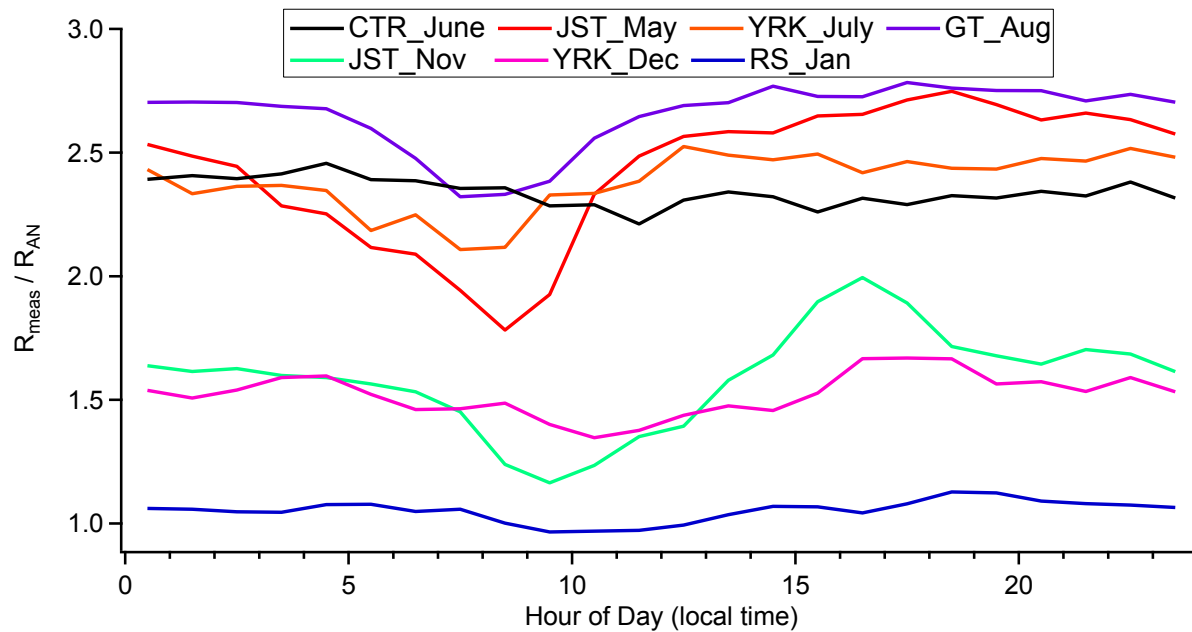
440

441

442

443

444 Fig. S15.



445

446

447

448

449

450

451

452

453

454

455

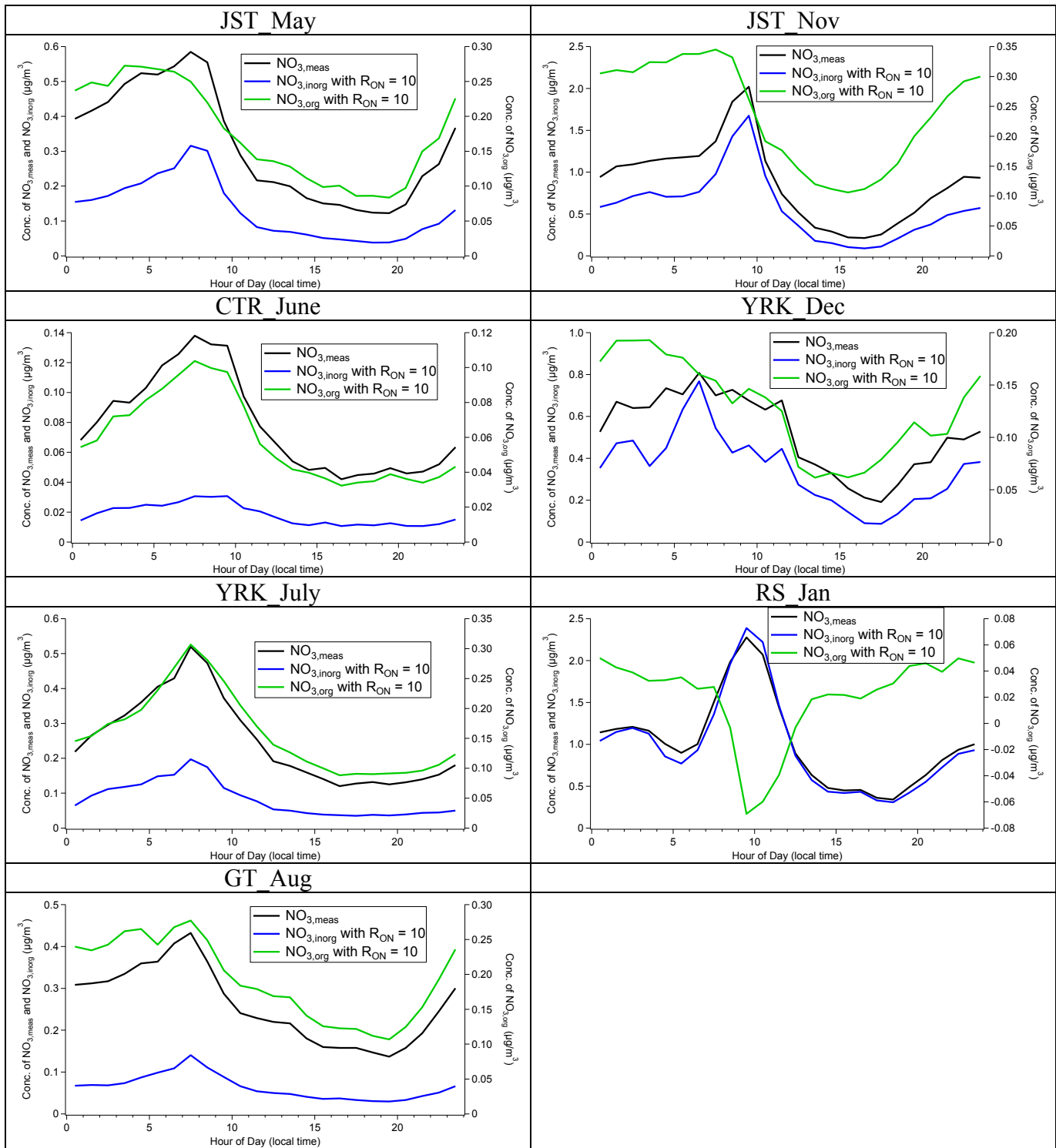
456

457

458

459

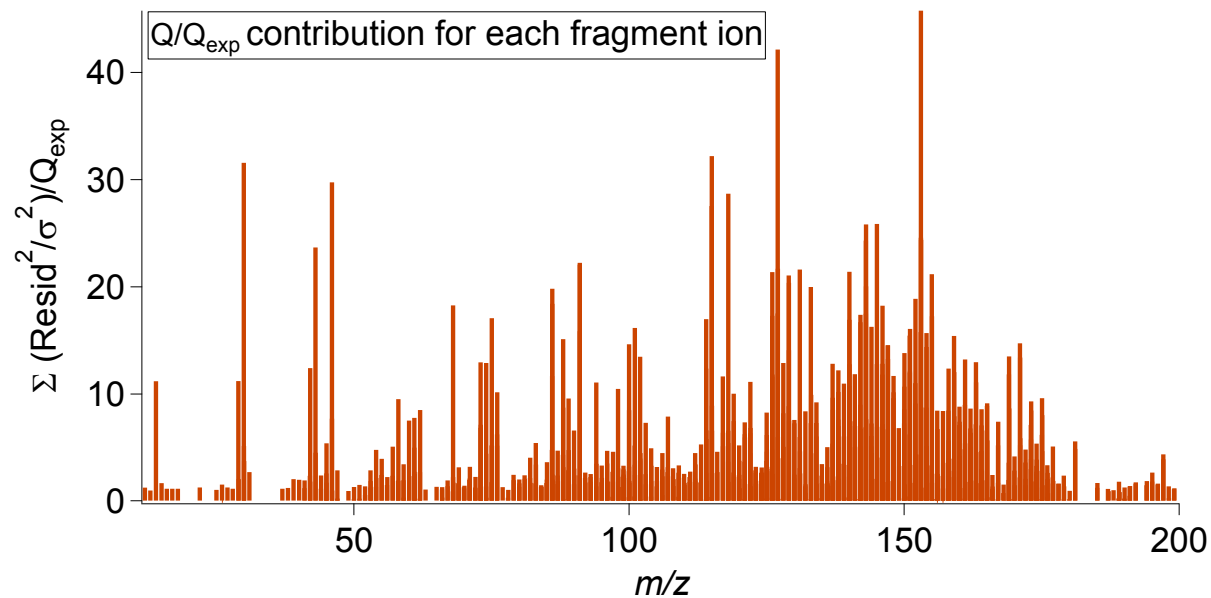
460 Fig. S16.



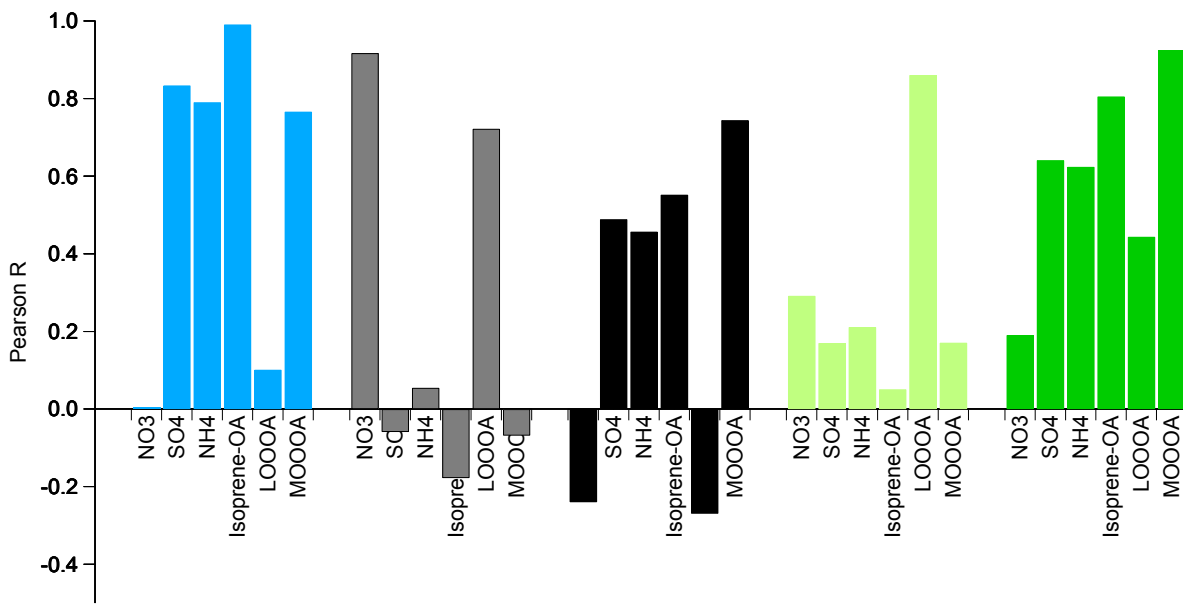
461

462

463 Fig. S17.



479 Fig. S18.



480

481

482

483

484

485

486

487

488

489

490

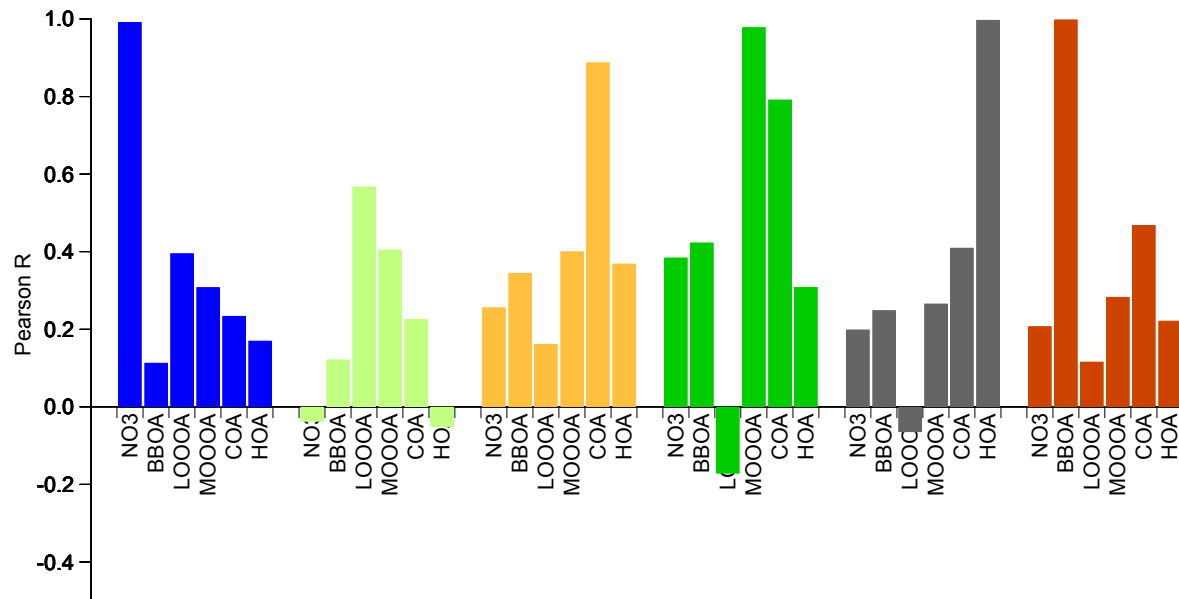
491

492

493

494

495 Fig. S19.



496

497

498

499

500

501

502

503

504

505

506

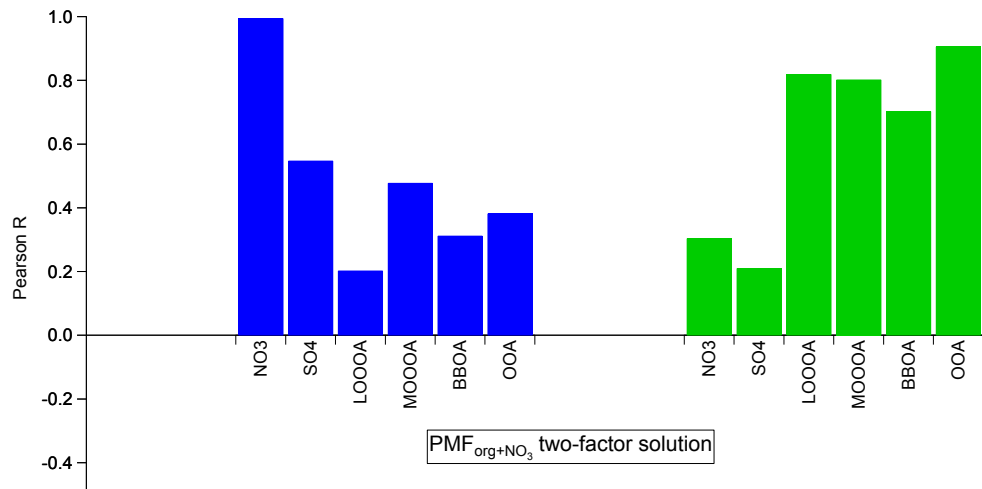
507

508

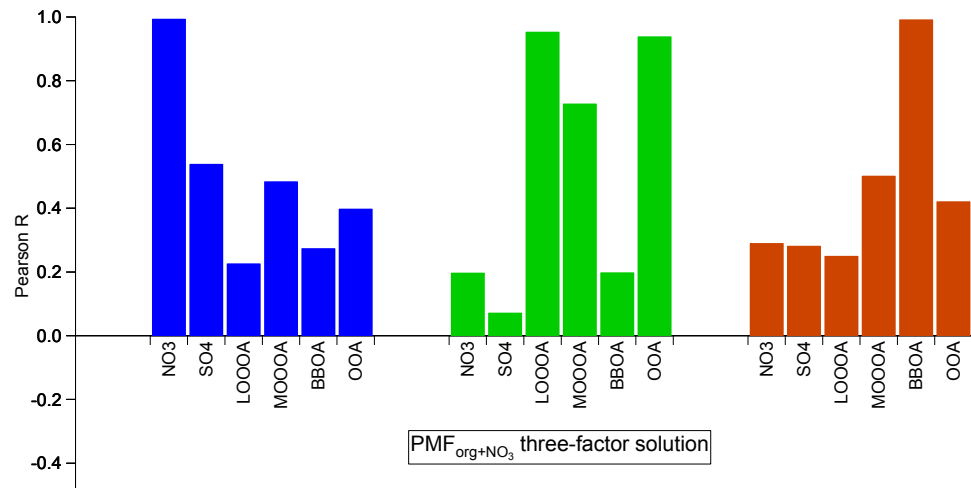
509

510

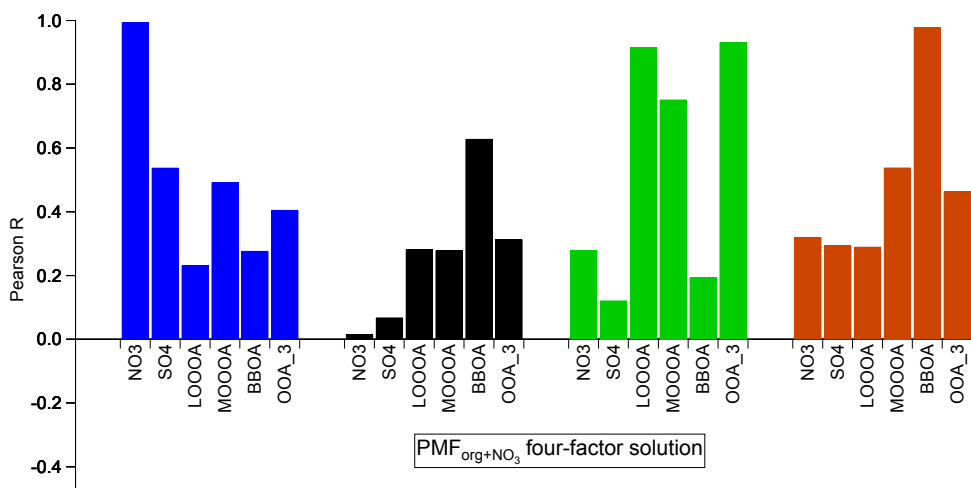
511 Fig. S20.



512



513



514

515 Reference

516

517 Ulbrich, I. M., Canagaratna, M. R., Zhang, Q., Worsnop, D. R., and Jimenez, J. L.: Interpretation  
518 of organic components from Positive Matrix Factorization of aerosol mass spectrometric data,  
519 Atmos. Chem. Phys., 9, 2891-2918, 10.5194/acp-9-2891-2009, 2009.

520